

# **An improved approach for cell traction force microscopy using a continuous hydrogel**

A thesis

Submitted to the faculty of

**WORCESTER POLYTECHNIC INSTITUTE**

In partial fulfillment of the requirements for the  
Degree of Master of Science

May 2013

Submitted by:       Mina Shojaei zadeh

Department of Physics

APPROVED BY:

---

Dr. Qi Wen, Thesis Adviser

---

Dr. David C. Medich, Master's Committee

---

Dr. Germano Iannacchione, Master's Committee & Department Head

## Contents

Acknowledgments .....	6
Abstract.....	7
1. Introduction .....	8
1.1. Cell mechano-transduction: .....	8
1.2. Traction force.....	10
1.3. Integrins .....	11
1.3.1. Integrins Structure .....	12
1.3.2. The structure of $\alpha$ subunit .....	13
1.3.3. The structure of $\beta$ subunit .....	14
1.3.4. Cation binding sites.....	15
1.3.5. Integrin – ligand partners .....	15
1.4. Methods of traction force measurements .....	17
1.4.1. CTFM using arrays of micro- or nano- pillars.....	17
1.4.2. CTFM methods using a continuous hydrogel .....	18
1.4.3. Shortcomings of current methods using a hydrogel .....	19
2. Method .....	21
2.1. PA gel .....	22
2.2. PA gel fabrication.....	22
2.3. Stiffness characterization .....	24
2.4. ECM ligands coating.....	24
2.5. Cell Culture .....	25
2.6. Traction force microscopy .....	25
2.7. Image analysis of the live cells.....	25
2.8. Pre-processing of images.....	28
2.8.1. Image Cropping.....	28
2.8.2. Drift removing.....	31
2.9. Determination of displacement fields .....	33
2.9.1 MATLAB Particle Tracking.....	33
2.9.2 MATLAB particle image velocimetry (MPIV) .....	34
2.9.3 Limitations of particle tracking .....	35

2.10. Finite Element analysis in ANSYS .....	40
2.10.1. The 3-D model for substrate.....	40
2.10.2. Determining nodal traction stresses.....	41
2.11. Post-processing.....	42
2.12. Validity of ANSYS model .....	45
2.13. Traction stress dependency on gel thickness .....	47
3. Results.....	48
3.1. Comparison of traditional method with the current method .....	48
3.2. CTF analysis results .....	49
3.3. Evaluating the effect of out-of-focus fluorescent beads .....	55
Conclusion and Future Works.....	59
4. Appendices.....	60
4.1. Appendix I- Pre-processing and post processing MATLAB codes.....	60
4.1.1. Pre-processing .....	60
4.1.2. Post-processing.....	64
4.2. Appendix II- ANSYS scripts .....	70
4.2.1. Model definition .....	70
4.2.2. Applying load on the gel .....	71
4.3. Appendix III-Tables: CTFs and cell areas.....	73
4.4. Appendix IV- Sample of analyzed cell images.....	75
References .....	78

## List of figures

Figure 1. The illustration of CTF in an adherent cell [15].....	9
Figure 2. 3T3 fibroblast morphological response to different extracellular matrix rigidity .....	11
Figure 3. Schematic of integrin heterodimer and its extracellular-intracellular domains .....	13
Figure 4. Integrin structure.....	14
Figure 5. Micro pillar posts on a PDMS substrate [28] .....	18
Figure 6. CTF measurement using a continuous hydrogel [31] .....	19
Figure 7. Fluorescent and phase images acquired from cell traction force microscopy: A) With the cell medium (force load), B)With Trypsin (null force), C) A color image of force load and null force overlaid , D) Phase contrast cell image.....	27
Figure 8. Displacement fields on different crop sizes: The largest A and the smallest D.....	30
Figure 9. Removing the microscope stage drift. Optical flow overlaid image (A) before and (B) after cropping and de-drifting the microscope drift with the cell boundary shown by red line .....	32
Figure 10. Comparison between PIV and Track. A) Red vectors PIV and blue vectors Track displacements. (B) Difference in pixel between PIV and Track along x- and y- axis .....	37
Figure 11. Aggregated beads and their intensity profile along x- and y- direction .....	38
Figure 12. Isolated beads with their intensity profile along x and y direction .....	39
Figure 13. Displacement fields and cell boundary on the cell phase image.....	39
Figure 14. Gel rectangular volume model in ANSYS with the cell (A) Top view, (B) Isometric view .....	43
Figure 15. Stress distribution with the cell boundary.....	44
Figure 16. Shear stress and shear stain .....	45
Figure 17. Total displacement on five cross sections of the gel when nodal uniform displacements (2 microns) were applied on the top .....	46
Figure 18. Total Stress change as a function of gel thickness.....	47
Figure 19. CTF and Cell area as a function of stiffness A) CTF [nN] B) Cell area[ $\mu\text{m}^2$ ] .....	52
Figure 20. Cell area as a function of CTF for A) Fibronectin and B) Collagen. ....	54
Figure 21. Density of fluorescent beads (out of focus) as a function of distance from the top in the gel. Y-axis the number of beads in distance z from the gel top. Zero corresponds to 50 micron (~1000 pixels) below the gel surface. The peak corresponds to the beads on the top layer.....	57
Figure 22. Stress distribution and traction force, replacing the displacement fields of the second layer on the top. ....	58
Figure 23. Phase image and tractional stress:Triangular shape cells .....	75
Figure 24. Phase image and tractional stress: Spindle shape cells.....	76
Figure 25. Phase image and tractional stress: Random or small triangular shape cells.....	77

## List of tables

Table 1. Effect of image cropping on CTF .....	29
Table 2. Comparison of traditional method by the novel method using experiments and simulation	49
Table 3. Average CTF and average area of the cells grown on fibronectin as well as on collagen on gel with stiffness 3.5, 7.5 and 20 kPa.....	53
Table 4. CTF and cell area for cells grown on 3.5, 7.5 and 20 kPa gel coated with fibronectin .....	73
Table 5. CTF and cell area for cells grown on 3.5, 7.5 and 20 kPa gel coated with collagen.....	74

## Acknowledgments

I would like to thank my advisor Dr. Qi Wen for his feedback, guidance and his patient throughout the course of my education and this project.

I would like to thank my thesis committee members Dr. Germano Iannacchione and Dr. David Medich for taking the time to help me through this final stage of my degree.

I would like to thank my lab mates Jared Franklin, Qian Xuyu and Gawain Thomas, for all of their assistance during the course of this project and the many endeavors outside of this project.

Finally but not least I would like to thank my family and friends for all their support, patience, and words of wisdom and encouragement that allowed me to keep everything in perspective throughout the course of my education.

## Abstract

In this thesis, a cell traction force microscopy method is developed for measuring traction forces of connective tissue cells. This method includes an improved methodology in traction force microscopy of live cells cultured on an elastic substrate. Tissue cells, such as skin and muscle cells respond to the mechanical stimuli of their microenvironment by adhering to their substrate and exerting forces on the proteins of the extracellular matrix (ECM). These forces are called cell traction forces. Fibroblasts are grown on polyacrylamide (PA) gels embedded with fluorescent beads and coated with different types of ECM ligands. Traction forces of NIH 3T3 fibroblasts are calculated from the measured deformations of PA gels by using a 3-D finite element method. The advantages of this method compared to the traditional methods of cell traction force microscopy (CTFM) are that this method takes into account the finite thickness of the substrate by applying a 3-D FEM analysis to reduce the errors of using an infinite half space approximation for a substrate with a finite thickness and that it uses a novel method for embedding the substrate with fluorescent markers that decreases the measurement uncertainties. In our approach fluorescent beads were embedded on the top of substrate instead of getting mixed with the gel. This decreases the effect of out-of-focus fluorescent beads on the measured deformation fields which enhances the accuracy of cell traction force measurements.

# 1. Introduction

## 1.1. Cell mechanotransduction:

Mechanotransduction is the mechanism by which cells convert mechanical signals into biochemical responses. By the other definition, mechanotransduction is the activation of cell surface receptors via extracellular or intracellular signaling molecule. Integrins, myosin motors, cytoskeletal filaments, nuclei and extracellular matrix are the factors that in concert have a significant contribution in mechanotransduction [1-2]. Previous studies suggest that mechanical properties of the cell microenvironment such as stiffness of the substrate could play an important role in generating the mechanical signals for cells. Many proteins associated with cell-Extracellular Matrix (ECM) adhesions; for example, integrins are a class of transmembrane receptors, responsible to transmit the mechanical signals from ECM to the cell. Integrins are one of the major receptors for signal transduction; there are, however, other types of receptors like cadherin transmit the signals between cells [3-4].

Mechanosensing has two major aspects: One is how the cell responds to external forces while and the other is related to the forces generated by the cell itself. Cells adhere to a substrate through focal adhesion sites on the cell surface (figure 1) which also enables them to receive the mechanical signals from their microenvironment. Specifically cells can sense the physical environment of the ECM, other cells in neighborhood and physical stress  $\tau$  by translating mechanical forces into biochemical signals. In response to these stimuli, cells exert internal forces generated in the cytoskeleton to the substrate. These forces are called traction forces.

The signal transduction between a cell and its microenvironment takes place through mechanotransduction and through cell surface transmembrane receptors. Therefore, the adhesive function of transmembrane receptors such as integrins and cadherins is a key element in mechanotransduction which means that study of their structure and how they transmit signals are important. Studies on the cells responses to the stiffness of the substrate indicates that cells adhere better and spread more on the stiff matrix, whereas on the soft substrate, their spreading area is smaller and cells maintain a round shape on the substrate [5-8]. Figure 2 shows NIH3T3 fibroblast morphological response to different matrix stiffness. The results suggest that cells respond to the stiffness of their substrate and, as the response, they change their stiffness to match that of their substrate. Cell rigidity is likely to be regulated by intracellular contractile force that causes the stiffening of the cell cytoskeleton. Therefore, cell traction forces indicate the cellular response to their microenvironments and hence studying them is of significant importance [9-10].

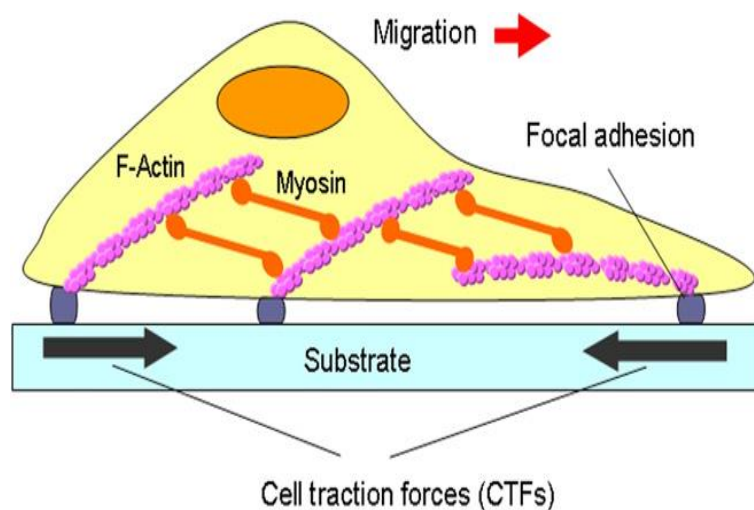
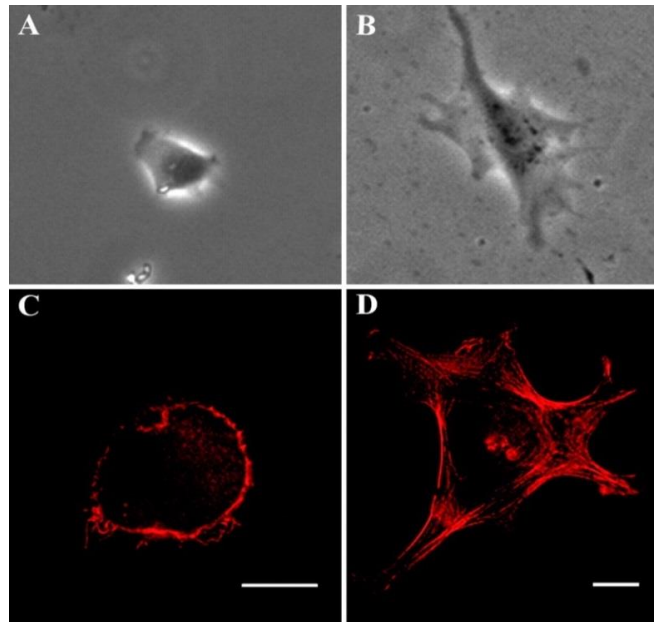


Figure 1. The illustration of CTF in an adherent cell [15]

## 1.2. Traction force

Most tissue cells such as skin, muscle and brain cells are not viable in fluids. In order to survive and grow, cells need to anchor on and spread over a substrate. As mentioned earlier, adherent cells generate internal traction forces (CTFs) on the substrate which are crucial in many vital cellular functions such as cell migration and mechanical signal transduction, as well as in many biological processes including inflammation, angiogenesis, and wound healing. There are two primary causes of traction force in the cell. One is the force generated by actomyosin interactions that cross-bridges between the actin bundles or stress fibers and hence generates tension that contracts the cell body (Figure 1) [10-11]. The second source of CTFs generation is through actin polymerization that gives rise to the forward locomotion of the cells, leading to the cell migration. CTFs are transmitted to the extracellular matrix (ECM) through stress fibers via focal adhesion. Focal adhesions (FA) are assemblies of ECM proteins, transmembrane receptors, and cytoplasmic structural and signaling proteins including integrins, paxilin and talin [12-14].



**Figure 2. 3T3 fibroblast morphological response to different extracellular matrix rigidity**  
**(A) & (B) are the phase image of the fibroblast on the soft and stiff gel. Cells on stiff gels are less rounded than those on the soft gel. Fluorescence images of fibroblasts on soft gel(C) and stiff gel (D) shows no stress fibers on the soft cell whereas stiff cells include bundles of actin filaments in their cytoskeleton [9].**

### 1.3. Integrins

Integrins are transmembrane receptors which mediate the attachment between a cell and its surroundings. They consist of  $\alpha$  and  $\beta$  subunits which are associated non-covalently [16]. Integrins attach to the ECM ligands on one side (the extracellular domain) and to the cell actin cytoskeleton (the integrin cytoplasmic tail) on other side; therefore, integrins mediate the adhesion between the cell cytoplasm and the cell microenvironment. In other words integrins pass the chemical and mechanical information of ECM to the cell cytoskeleton (outside-in signaling) and from the cell cytoskeleton to the ECM or other cells (inside-out signaling) [17].

In order to transmit the mechanical forces; integrins undergo conformational changes in their extracellular domain to regulate their attachment to extracellular matrix ligands. This

conformational change is the response of the integrin to the signals that are imposed from the integrin cytoplasmic tail [18].

Hence, by binding both extracellular and intracellular ligands, integrins provide a transmembrane link for the bidirectional transmission of mechanical force and biochemical signals across the plasma membrane. Proteins such as talin play an important role in integrin activation [18]. They interact with integrin  $\beta$  subunit to activate integrin and hence transmit the signals into ECM.

An important characteristic of integrins is that they bind to a variety of ligands; yet each type of ligands also can activate different types of integrins. For instance, collagen activates  $\alpha 1\beta 1$  and  $\alpha 2\beta 1$  integrins, and fibronectin can activate  $\alpha 5\beta 1$ ,  $\alpha 8 \beta 1$  and,  $\alpha V\beta 1$  integrins [19]

### **1.3.1. Integrins Structure**

All integrins contain an  $\alpha$  and a  $\beta$  subunit. The  $\alpha$ - and  $\beta$ - subunits are constructed from several domains with flexible linkers between them.  $\alpha$  - and  $\beta$  -subunits contain around 1000 and 750 amino acids, respectively. Mammalian genomes contain 18  $\alpha$  subunit and 8  $\beta$  subunit genes. These subunits assemble into 24 different  $\alpha$ - $\beta$  receptor combinations with different binding properties [20].

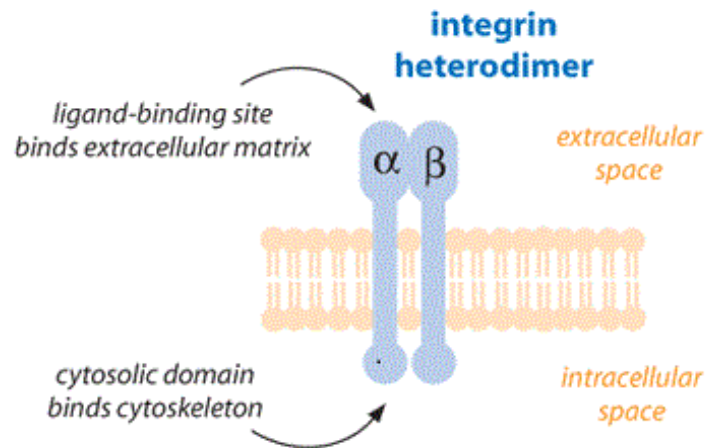
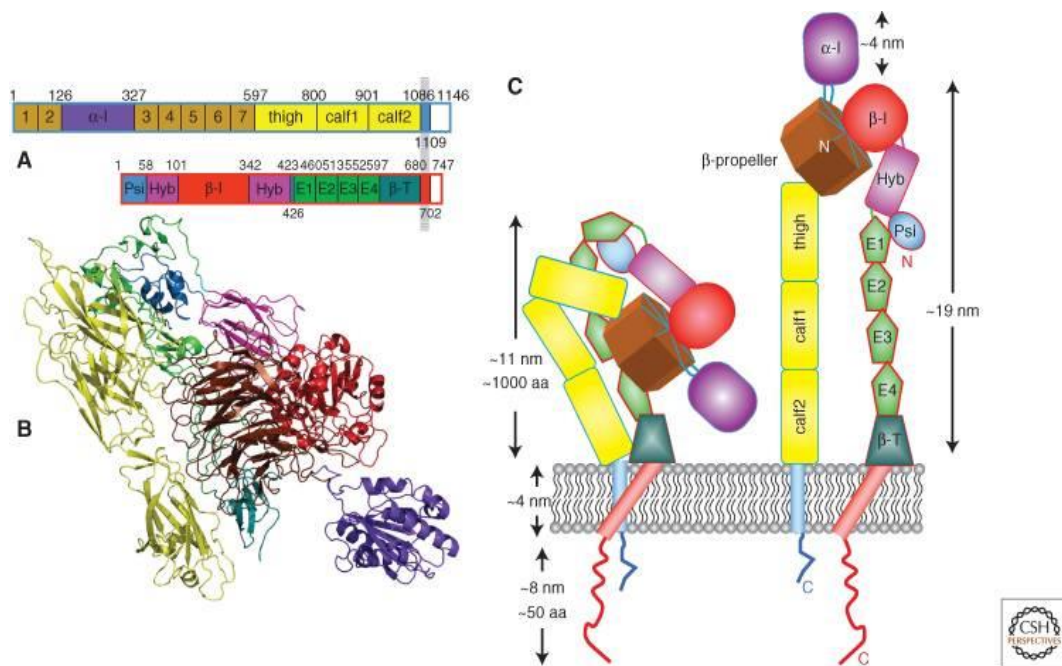


Figure 3. Schematic of integrin heterodimer and its extracellular-intracellular domains (<http://www.scq.ubc.ca/the-role-of-integrins-in-wound-healing>)

### 1.3.2. The structure of $\alpha$ subunit

The structure of  $\alpha$  subunit is represented in Figure 4.C  $\alpha$  subunit [21-22]:

- Consists of four or five extracellular domains: a seven-bladed  $\beta$ -propeller, a thigh, and two calf domains (Calf 1 and Calf2),
- These domains are followed by a single transmembrane helix and a small cytoplasmic domain.
- Nine of 18 integrin  $\alpha$  chains have an  $\alpha$ -I or  $\alpha$ A domain of around 200 amino-acids, inserted between blades 2 and 3 of the  $\beta$ - propeller
- The I domain has five  $\beta$ -sheets surrounded by seven  $\alpha$  helices



**Figure 4. Integrin structure**

**(A) Domain structure of  $\alpha\beta 2$ ; (B) structure of  $\alpha\beta 2$  using same color code as A; (C) cartoon representation of bent and upright conformations showing approximate dimensions [23]**

### 1.3.3. The structure of $\beta$ subunit

The structure of  $\beta$  -subunit is also indicated in Figure 4.C and consists of [22]:

- Seven domains with flexible and complex interconnections.
- A  $\beta$ -I domain is inserted in a hybrid domain
- An N-terminal Plexin-semaphorin-integrin (PSI) domain which is linked via an S-S bond to EGF1(cysteine-rich epidermal growth factor) domain
- C-terminal of the hybrid are four EGF-like domains (EGF1-4)
- A  $\beta$ -tail domain followed by transmembrane helix and cytoplasmic domain
- $\beta$  -I domain is homologous to the  $\alpha$ -I domain
- $\beta$  -leg seems to be more flexible than the  $\alpha$ -leg domain

#### 1.3.4. Cation binding sites

The last three or four blades of the  $\beta$ -propeller contain domains that bind  $\text{Ca}^{2+}$  on the lower side of the blade and binding of  $\text{Ca}^{2+}$  to these sites influences ligand binding. In integrins with no  $\alpha$ -I, the ligand binds at the largest interface between the two subunits (the  $\beta$ -propeller /  $\beta$ -I domain interface) and binding is dependent on the cations  $\text{Mg}^{2+}$ ,  $\text{Ca}^{2+}$ , and  $\text{Mn}^{2+}$ .

Integrin ligand binding involves an  $\text{Mg}^{2+}$  ion, a “metal-ion-dependent adhesion site” (MIDAS). Three  $\beta$ -I domain metal-binding sites in  $\alpha\text{X}\beta 2$  are; MIDAS, ADMIDAS and SYMBS (synergistic metal ion binding site).  $\text{Mg}^{2+}$  is assigned to central MIDAS and  $\text{Ca}^{2+}$  is assigned to ADMIDAS and SYMBS [22-23].

#### 1.3.5. Integrin – ligand partners

Despite their wide variety, integrin-ligand combinations are clustered into four main groups [23-24]:

- 1) RGD-binding integrins: Integrins such as  $\alpha\text{V}\beta 1$ ,  $\alpha\text{V}\beta 3$ , and  $\alpha 5\beta 1$  are able to bind to the ligands with an RGD tripeptide active site. RGD binds at an interface between  $\alpha$  and  $\beta$  subunits. Fibronectin activates  $\alpha 5\beta 1$ ,  $\alpha 8 \beta 1$ ,  $\alpha\text{V}\beta 1$ ,  $\alpha\text{V}\beta 6$ ,  $\alpha\text{V}\beta 3$ ,  $\text{IIB}\beta 3$  integrins by its RGD binding site which is an acidic motif LDV peptides like RGD bind to the integrins at the junction between  $\alpha$  and  $\beta$  subunits.
- 2) LDV-binding integrins:  $\alpha 4\beta 1$ ,  $\alpha 4\beta 7$ ,  $\alpha 9\beta 1$ , etc. are integrins that bind to ligands with LDV binding site which is an acidic motif. LDV peptides like RGD bind to the integrins at the junction between  $\alpha$  and  $\beta$  subunits. Fibronectin type III contains the LDV binding site that binds to integrins  $\alpha 4\beta 1$  and  $\alpha 4\beta 7$ .

- 3)  $\alpha$ A – domain –  $\beta$ 1 integrins ; Collagen and laminin are the ligands that contain this binding site. Four  $\alpha$  subunits containing  $\alpha$ A-domain ( $\alpha$  1,  $\alpha$  2,  $\alpha$ 10 and  $\alpha$ 11) combine with  $\beta$  1 and form a distinct laminin/collagen subfamily:  $\alpha$ 1 $\beta$ 1,  $\alpha$ 2 $\beta$ 1-  $\alpha$ 10 $\beta$ 1-  $\alpha$ 11 $\beta$ 1
- 4) Non –  $\alpha$ A – domain integrins;  $\alpha$ 3 $\beta$ 1,  $\alpha$ 6 $\beta$ 1 have no  $\alpha$  A domain and are highly selective laminin receptors

## 1.4. Methods of traction force measurements

Cellular response determines whether or not a cell is able to accomplish its vital biological functions. Cancer or unhealthy cells could be recognized via their different behavior or morphology from healthy cells. Thus, developing novel methods which are able to measure the exact amount of cellular forces as the response to mechanical stimuli are important. So far, different methods have been developed to measure the CTFs of single cells as well as a population of cells. Numerous approaches for measuring CTFs have been developed due to the advances in micro- and nanotechnology; these methods include Cell-populated collagen gel (CPCG), and Traction force microscopy (CTFM) using a flat elastic substrate (Figure 6), such as hydrogels of polyacrylamide (PA) or arrays of micro- or nano-pillars (Figure 5) made of Polydimethylsiloxane (PDMS) [25-29].

### 1.4.1. CTFM using arrays of micro- or nano- pillars

Tan et al. measured cellular traction forces using polydimethylsiloxane (PDMS)-based elastic substrates with a micropillar array for the first time. Traction forces  $F$  were determined using the equation  $F = k \delta$ , where  $k$  and  $\delta$  are the spring constant and deflection of the micropillars. The spring constant of the pillars  $k$  was obtained from Young's modulus of the substrate and the pillar geometry. However, the stiffness of PDMS substrate cannot be adjusted low enough to sense small deformations [29].

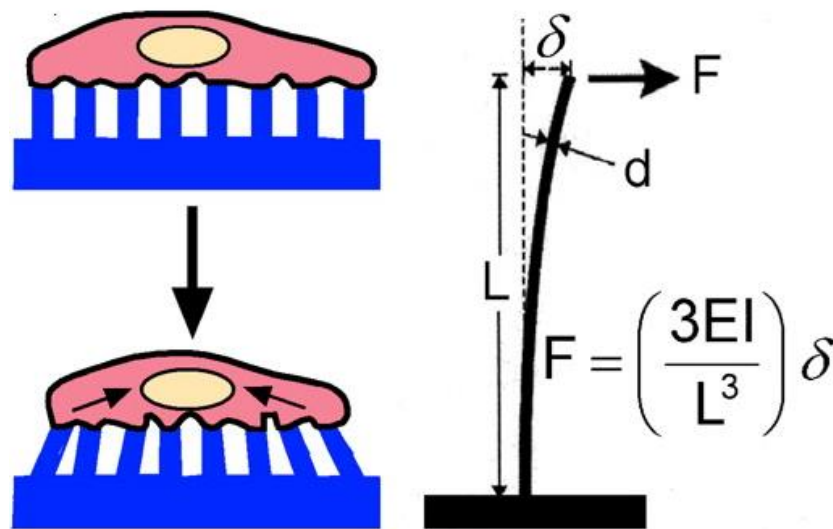


Figure 5. Micro pillar posts on a PDMS substrate [28]  
 The spring constant depends on the micro-pillar geometry, moment of inertia  $I$ , and elasticity of micro-pillar  $E$

#### 1.4.2. CTFM methods using a continuous hydrogel

Using a PA gel as the flexible substrate, different groups such as Dembo and Wang (DW) [30], Butler et al [31] and Yang et al. [32] have developed new approaches to measure CTF of tissue cells. There are three primary steps to measure the CTF in all TFM methods. The first step is to fabricate the elastic substrate which is a polyacrylamide gel with embedded fluorescent beads. The second step is to compute the bead displacements on the substrate from a pair of “null-force” and “force-loaded” images, and the third step is to determine the cell traction forces from the substrate displacements. The first step is common to all methods, but the second and third steps may differ [9].

Cell traction force microscopy using a hydrogel is now among the most efficient methods for determining traction forces of the cells adhering to the surface of the elastic substrate due to the advantages that they provide. Using Polyacrylamide (PA) gel as a substrate retains

advantages compared to the other methods because PA gels are highly elastic, transparent, mechanically stable and easy to prepare. In addition, the stiffness of PA gels is tunable by changing the ratio of base to cross linker in the stock solution hence producing gels with varying Young's modulus. These properties also make PA gel an excellent substrate for CTFM methods. Therefore, we performed a cell traction force microscopy of cells grown on a hydrogel. Although this CTFM method has many advantages compared to the other methods, there are still some limitations regarding the CTFM method using a continuous hydrogel which is described in the following paragraph.

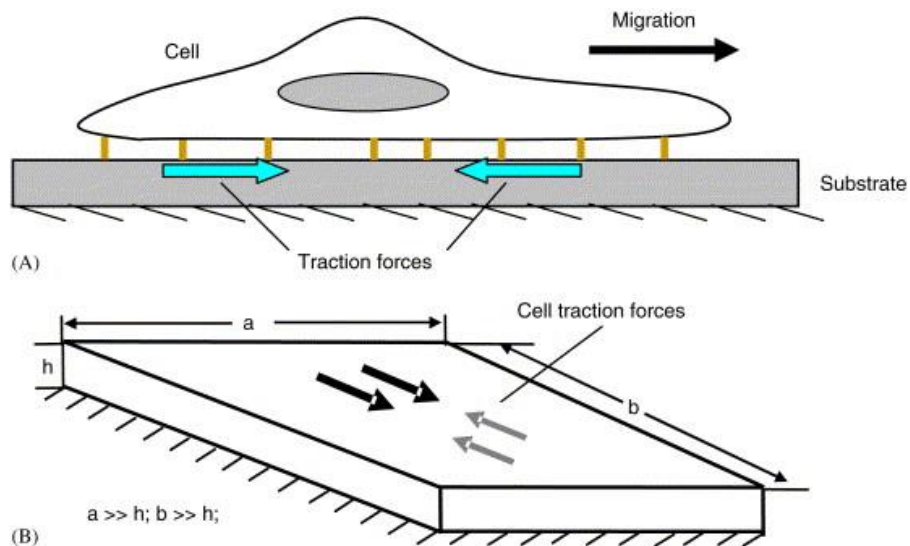


Figure 6. CTF measurement using a continuous hydrogel [31]

### 1.4.3. Shortcomings of current methods using a hydrogel

The problems with the current hydrogel method includes 1) embedding the fluorescent beads within the gel solution and 2) considering the thin polyacrylamide substrate to be an infinite half-space in order to use the Boussinesq analytical solution (DW and Butler et al) .

Cells are grown on the gel with finite volume and finite thickness; therefore, considering an infinite half-space model introduces errors. Yang et al. evaluated this error [31]. They assessed the effect of substrate thickness on an induced point surface load. They found that using Boussinesq solution for infinite half-space approximation generated larger errors for gel thicknesses of 70 and 200  $\mu\text{m}$ , while this approximation worked well for gel with 1000  $\mu\text{m}$  thickness. Therefore, for a finite thickness of substrate the Boussinesq solution does not work well.

To overcome this limitation and, in order to take the finite thickness of gel into account, we applied a 3-D finite element method analysis (FEM) in ANSYS. In this FEM analysis, substrate is modeled as a rectangular volume with the dimension of the fluorescent images and a height approximately equal to the gel thickness. The significant purpose of this project is to develop methods to limit the beads on the gel top instead of mixing them with the gel and hence increase the accuracy of measurements. Therefore, we coated the gel with the beads on the gel surface. It is shown later that embedding the beads on the top increases the accuracy of CTF results; however, some beads go into the gel and will not remain on the top. These beads are out of the microscope focus and reduce the accuracy of CTF measurements. Our next purpose is to develop methods to precisely evaluate the effect of beads out of focus on the results and hence improve the accuracy of results based on this evaluation.

## 2. Method

PA gels with varying stiffness from 3.5 kPa to 20 kPa were made changing the ratio of base to cross linkers. Then fluorescent beads were coated on the gel top 3T3 fibroblast cells were then grown on the substrate. A fluorescent microscope was used to take the images of the substrate with cell after the cell was detached from the substrate. Displacement fields due to small movements of the fluorescent beads on gel were then calculated by correlating the fluorescent images using the MATLAB image processing toolbox. A 3-D Finite element analysis of the gel with the displacements on the top was then applied to calculate the stress due to the cell contractile force. Further experiments and analysis were performed to validate the model and evaluate the accuracy of results by evaluating the effect of out-of-focus beads.

## 2.1. PA gel

Polyacrylamide gels are well known to be one of the commonly used substrate to measure the CTFs. The gel surface is inert and non-adherent to the cell surface receptors and the other proteins of the cell. Thus, only the ligands can bind to the surface with the covalent bonds. These characteristic enable PA gel to be a proper material for studying the effect of ligands on cellular responses [33-34]

The other advantage of PA gels is that their stiffness is tunable through changing the concentration of acrylamide to bis-acrylamide (base to cross-linker) in the solution, allowing for control over the substrate stiffness. The first usage of PA gels as cell culture substrate was in 1978 [35]; however, the first study using PA gels of different stiffness was undertaken by Pelham and Wang [36].

The substrate material is presumed to be isotropic, meaning its properties are the same in all directions. The substrate can be mathematically modeled with Hooke's law as a spring with a spring constant  $k$  that exerts a force  $F$  proportional to the distance,  $x$ , by which it is extended, following the expression  $F = -kx$ . The spring constant,  $k$ , is related to the material's shear modulus, a constant for the material that describes its resistance to shear, expressed as stress over strain.

## 2.2. PA gel fabrication

PA gels were prepared and made on the cover slip glasses in order to make a flat surface of the gel. The glass surface must be prepared and activated to bind to the gel. 25x25 mm cover glasses were soaked in ethanol and cleaned with a sonicator for five minutes, and

the plasma cleaned with a SPI Supplies Plasma Prep II machine. Then they were placed in a 10% (3-Aminopropyl) trimethoxysilane aqueous solution with a stir bar and were stirred for 30 minutes. After this time, the slides were flushed with distilled water and heated in an oven until all water had evaporated. The slides were then allowed to dry and were placed in a Glutaraldehyde bath and refrigerated for three hours.

The other glasses with the same size were soaked in ethanol and cleaned with a sonicator for five minutes. Next they were dried and plasma treated for 45 seconds. The slides were then each coated with 50  $\mu$ l of the 0.5% bead solution in order to cover the whole glass surface with a favorable concentration of beads. The glasses were immediately placed in an oven at 150°C in order to rapidly evaporate the ethanol to prevent the beads aggregation. The bead solution was made using ethanol and 0.2  $\mu$ m diameter red fluorescent carboxylate-modified microbeads.

Polyacrylamide solution was made by mixing acrylamide with N, N-methylene-BIS-acrylamide (BIS) and HEPES buffer. Gels with different stiffness were made by changing the concentration of BIS and hence changing the ratio of acrylamide to BIS concentration (base to cross-linker). The acrylamide/BIS solutions prepared were 5% PA 0.1% Bis, 8% PA 0.1% Bis, and 12% PA 0.14% Bis. The solution was polymerized by adding 2.5  $\mu$ l of ammonium persulfate and 0.9  $\mu$ l of tetramethyl ethylenediamine (TEMED) to 250 microliter of the solution. 64  $\mu$ l of the gel solution were dropped on the bead-coated surface of a slide, and then a glutaraldehyde-treated slide was positioned on top of the surface. After seven minutes, the slides were pried apart, resulting in a solidified gel adhering to the glutaraldehyde-treated

slide. The gels were kept moisturized with HEPES buffer solution. Gels were glued into petri dishes and kept moist with HEPES buffer.

### **2.3. Stiffness characterization**

The stiffness of the polyacrylamide gels was characterized by microindentation using an atomic force microscope. The cantilevers used were model DNP-D (Bruker, USA) with a force constant of 0.06 – 0.1 N/m. After calibrating the cantilever for the spring constant and deflection sensitivity, indentation was performed using an approach velocity of 10  $\mu\text{m/s}$  and a maximum deflection (trigger point) of 50 nm. The acquired force curves were fitted to the Hertz model to determine the elastic modulus.

### **2.4. ECM ligands coating**

A solution was made using 1mg of sulfo-sanpah, [30], 8 microliters of dimethyl siloxide, and 1000 microliters of HEPES buffer. Buffer was aspirated from the gels and in order to activate the polyacrylamide 250 microliters of sulfo-sanpah solution was pipetted onto each gel. The gels were left in a sterile hood with UV light shining on them for 10 minutes in order to bind the sulfo-sanpah to the gel surfaces. The gels were then rinsed with HEPES buffer 5 times in order to remove any excess sulfo-sanpah. Next, a 0.1 mg/mL collagen solution was prepared in HEPES buffer and 50 microliters of the solution was pipetted onto each gel. The collagen was allowed to settle on the gel surfaces for 1 hour. After this time, the gels were once again rinsed with HEPES buffer 5 times in order to remove excess collagen, and then were submerged in HEPES and stored in a refrigerator until cells were ready to be seeded on the gels. Fibronectin was coated on the gel with the similar protocol.

## 2.5. Cell Culture

NIH 3T3 fibroblasts were maintained at 37°C and 5% CO<sub>2</sub> in Dulbecco's Modified Eagle's Medium supplemented with 10% Fetal Bovine Serum and 1% penicillin-streptomycin. Cells were left for one day to grow.

## 2.6. Traction force microscopy

Cells were seeded onto the gels at a low concentration and left to incubate overnight. The next day, cell images were taken using a Zeiss Axiovert 200M Microscope. Healthy, isolated cells were imaged at 40x magnification and red fluorescence was used to capture images of the microbeads below them. After the initial images were taken, the cell medium was extracted from the petri dish and replaced with phosphate-buffered saline. After several minutes, images were taken again. The PBS was extracted and replaced with 0.5% trypsin. The trypsin was reapplied until all selected cells had been removed from the gel surface. Images were then taken of the positions where the cells had formerly been, so that the bead positions with and without cell traction force applied could be compared.

## 2.7. Image analysis of the live cells

The traction stresses generated by the cells are transmitted to the substrate, causing small movements of the beads. The fluorescent beads are used as the markers for tracking the drift on the gel under the cell. Fluorescent images of the gel with microbead markers are taken before and after cells were detached from ECM with trypsin. This image change from “load” (with cell medium) to “relax” (with trypsin) image is called Optical Flow [37]. Each pixel on an image has a gray value determined by an 8-bit integer. MATLAB image processing tools are used to read and analyze these images. Figure 5 shows the sets of images were analyzed.

Figure 7.A is the fluorescent image of the substrate with the fluorescent markers with the cell medium (load) and Figure 7.B is the substrate with trypsin (relax). Figure 7.C represents an overlaid RGB image of their optical flow. This image indicates how the beads are drifted from their positions on image 7.A to those on image 7.B and Figure 7.D is the phase contrast cell image.

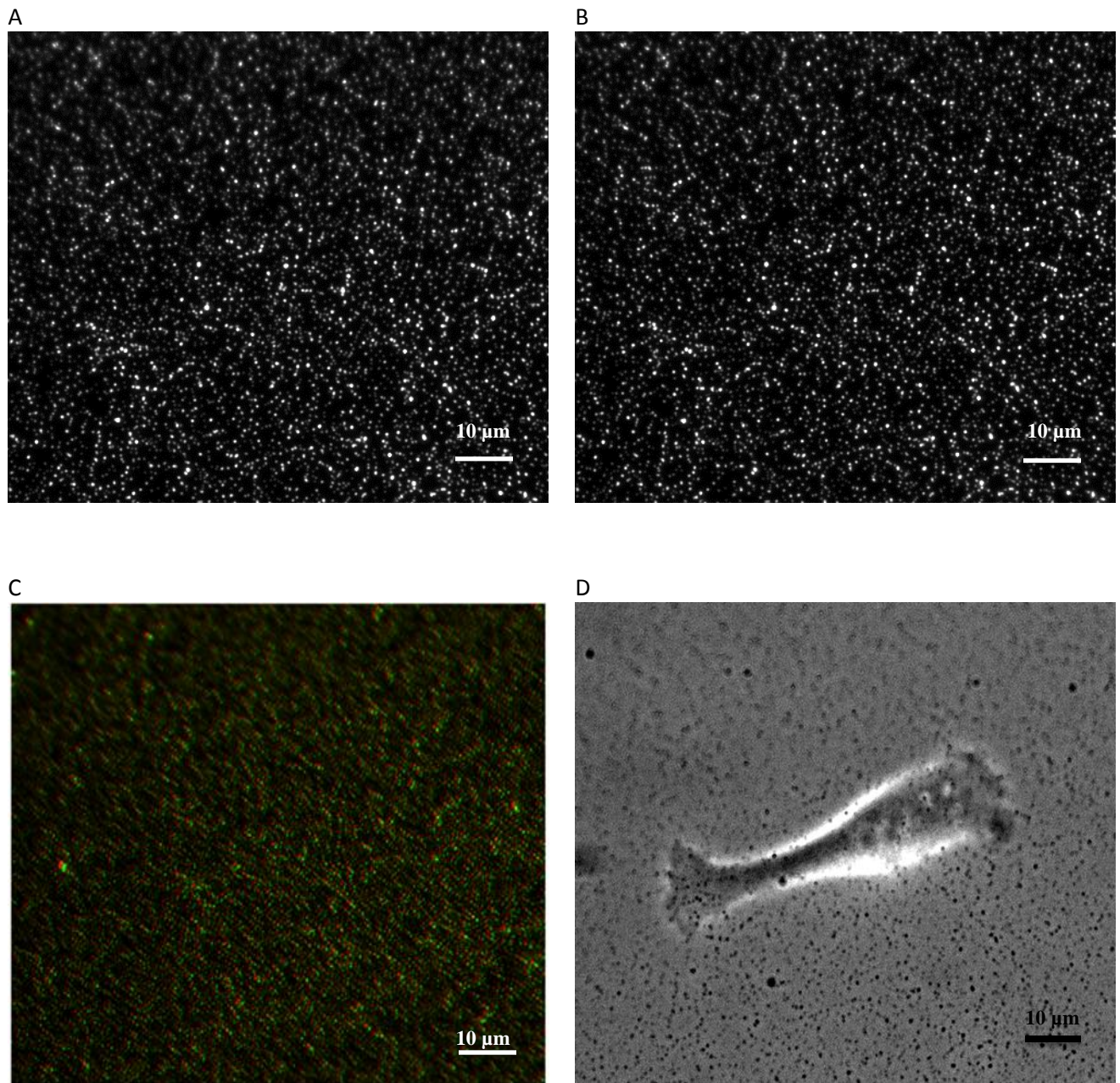


Figure 7. Fluorescent and phase images acquired from cell traction force microscopy: A) With the cell medium (force load), B)With Trypsin (null force), C) A color image of force load and null force overlaid , D) Phase contrast cell image

## 2.8. Pre-processing of images

The original size of the images in Figure 7 is (1030 × 918 pixels); However, before performing further analysis in MATLAB and ANSYS, the images were cropped within a smaller area including and slightly greater than the cell boundary for to shorten the analysis time by analyzing smaller windows of images and to consequently reduce the errors due to the measurements. Cells apply traction force on the underlying substrate; however, this force is restricted to a small area around the cell boundary which enables us to precisely measure the traction force of individual cells.

In addition, microscope objective position was changed across the dish to find the healthy cells and acquire the force load images. In order to acquire the null force images, the microscope objective was then returned to the original cell positions after dissociating the cells from ECM. This process results in a small drift between the optical flow images. This drift was calculated and then removed from the total displacements in order to acquire the actual displacement due to the cell traction. The image cropping and drift removing (de-drifting) process is described as the following.

### 2.8.1. Image Cropping

To evaluate the effect of cropping on the CTF results and to determine the minimum size for cropping, CTFs were measured for different cropped areas by our method described in the current chapter. The results of four different cropped areas are indicated in table 1. CTF changes slightly by increasing the cropping area. Furthermore, figure 8 shows different crops (A-D). None of these areas are proper for cropping as A is very large and hence results in a long time analysis, and D is very small that results in losing the displacements fields next

to the cell edges. Therefore, the cropping area size must be between these two sizes, in order not to lose the traction forces corresponding to CTF at the edges. B or C crop size appears to be the proper sizes for cropping considering the slight changes in traction forces between them. Therefore, when cropping the images the sizes must be large enough to include the traction displacements around the cell edge, but not too large to result in increase in the analysis time.

**Table 1. Effect of image cropping on CTF**

<b>Crop</b>	<b>1</b>	<b>2</b>	<b>3</b>	<b>4</b>
<b>CTF [nN]</b>	321	300	275	250
<b>Cropped Area [pixel<sup>2</sup>]</b>	477365	270865	149265	96240

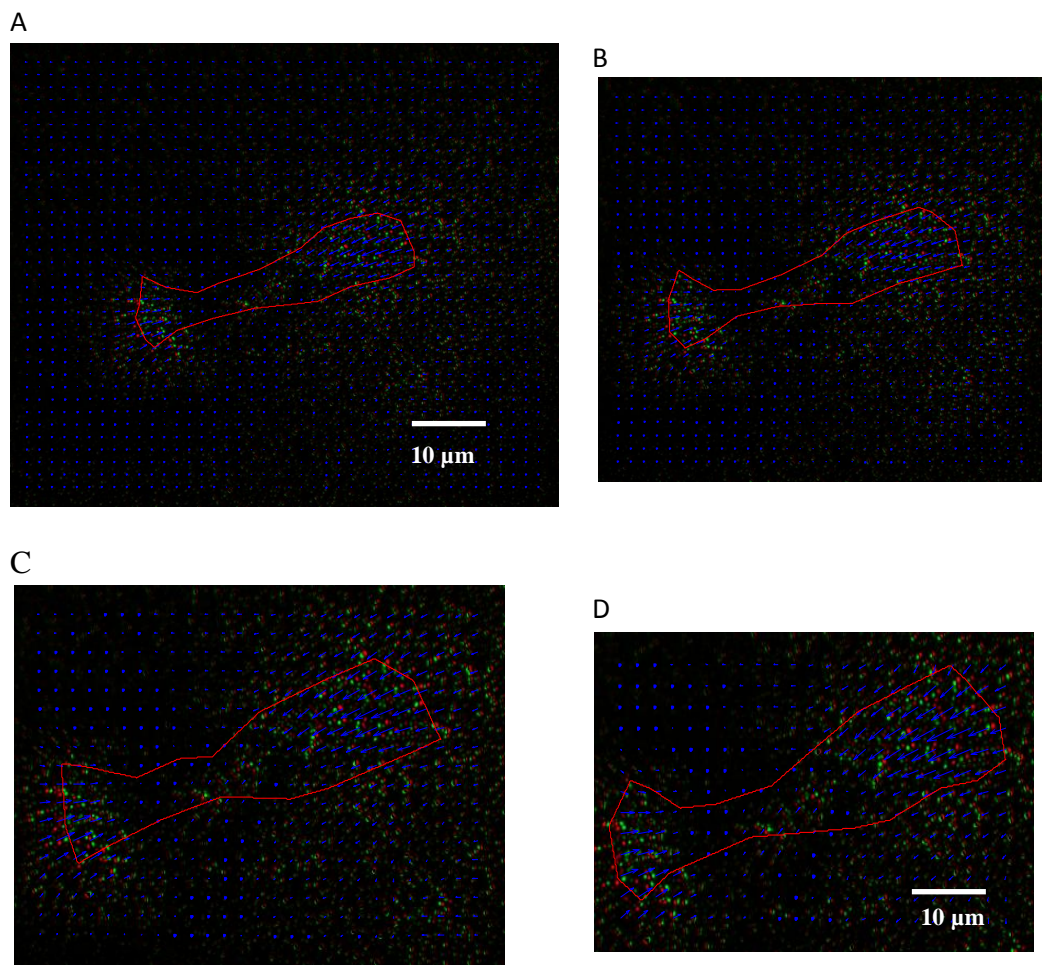
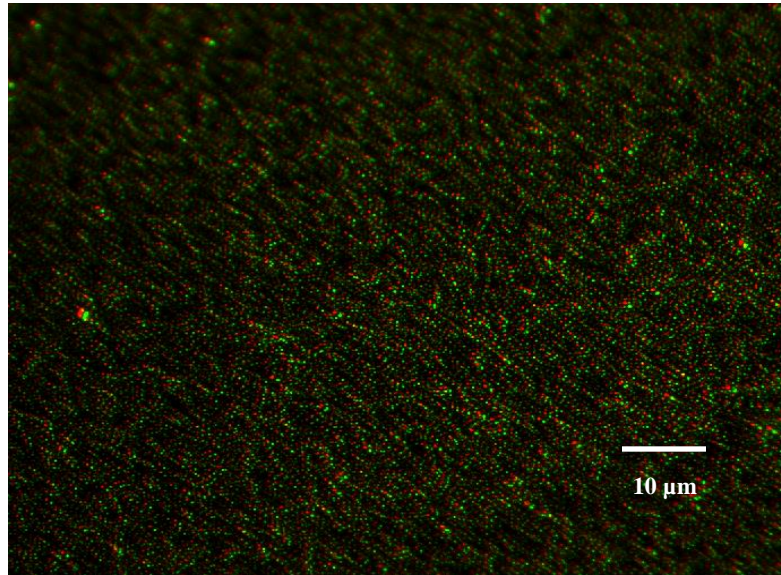


Figure 8. Displacement fields on different crop sizes: The largest A and the smallest D

### 2.8.2. Drift removing

To find the drift of the microscope stage four corners on the cell phase image were selected. These regions were picked because the cell traction force does not apply on the distances far from the cell territory; meaning that on the image corners, displacement vectors are merely due to the microscope stage drift, while at the cell boundary; displacement vectors are due to both traction forces and microscope stage drift. This drift was then calculated by cross-correlating the null force and the force load images and then taking the average of the displacements computed in these regions. The average was then subtracted from the bead's location on the force load image or was added to those on the null load image. This process was called as de-drifting or drifts removing process. Figure 9.A, B indicates the optical flow overlaid images before and after de-drifting respectively. The cell boundary is also plotted on the image to show the area involved in the CTF. Figure 9.B shows how the cell is displacing the substrate. Once the drift is found, the phase contrast image is cropped by the area around cell region. The null force and force load images are cropped correspondingly. Having the fluorescent images de-drifted and cropped, the next step is to find the displacement fields that the movement of beads generates on gel.

**A**



**B**

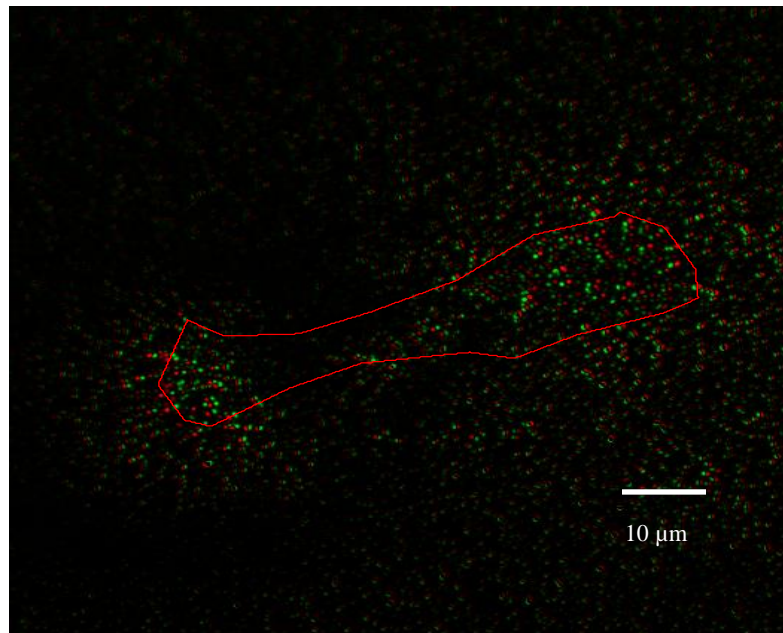


**Figure 9.** Removing the microscope stage drift. Optical flow overlaid image (A) before and (B) after cropping and de-drifting the microscope drift with the cell boundary shown by red line

## 2.9. Determination of displacement fields

To determine the displacement fields due to the small movements of the fluorescent beads, two different analysis methods were applied on the cropped and the de-drifted images of null load and force load. The first method applied was using MATLAB Particle Tracking toolbox and the second one was using MATLAB Particle Image Velocimetry (MPIV). Then, the results were compared with further analysis to evaluate the limitations of these methods and selecting the one which is more accurate.

In Particle Tracking method, MATLAB functions are used to track the beads location from null force image to force load image. In PIV, the particles are not tracked, however, and are instead cross-correlated from relax to load image. These methods are described in details in the following.

### 2.9.1 MATLAB Particle Tracking

MATLAB functions used in this toolbox are: `bpass.m`, `pkfnd.m` and `cntrd.m` developed by Daniel Blair and Eric Dufresne. The first step in this process is to spatially filter the images. First the images are spatially filtered by a function called “`bpass`” which is a spatial bandpass filter that smooths the image and subtracts the background. Inputs of `bpass` are the images and the diameter of the particles in pixels. Diameter value could be manipulated, in order to acquire an image with clear circular blobs (fluorescent beads). “`bpass`” outputs the position of these blobs. The next step is to identify the blobs that “`bpass`” has found as the particles. Given the threshold value and the diameter of the blobs “`pkfnd`” function finds the location of all of the peaks that are above the given threshold value. This function provides a first estimate of particle locations to “pixel-level accuracy”. Another function called “`cntrd`” is

then used to find a more precise location of the particles. The exact locations of the center of the particles whose intensity are above the defined threshold value are detected. The last or the most important step is to track the beads whose locations have been detected using a function called “track”. The inputs of Track include a matrix made of position of beads locations and the beads labels. The second input has to be a value smaller than the mean inter particle separation. Mean inter particle separation is calculated using the following formula

$$P(r) = \frac{N(r)}{2\pi\Delta r} \quad (2.2)$$

where  $P(r)$  is the probability distribution function of distance to the nearest neighbor particle.  $N(r)$  is the number of beads in distance  $r$  from center of a bead. This value is found by plotting the histogram of distance calculated for each bead from other beads and  $\Delta r$  is the bin. Mean inter particle distance is the distance at which the average  $P(r)$  value is maximum. Track function tracked the beads’ movements and found the displacements. These beads have moved from  $(x_{1i}, y_{1i})$  in the “null load” image to  $(x_{2i}, y_{2i})$  positions in the “force load” image. The output is a matrix that includes the beads number, beads locations, and their corresponding displacement fields. Track function tracks the beads whose displacements are smaller than their separation from the closest neighbors.

### 2.9.2 MATLAB particle image velocimetry (MPIV)

MPIV is the particle image velocimetry (PIV) toolbox written in MATLAB by Nobuhito Mori (Osaka City University, Japan) and Kuang-An Chang (Texas A&M University). We used MQD (minimum Quadratic Difference) algorithm in the program to find the displacements vectors. Input variables for the MPIV function are: Two images with the

double precision, window size that should be larger than 20 pixels, and maximum and minimum displacement along x- and y-direction in pixels. In the program the ratio of the values of the highest peak to the second highest peak and the ratio of the values of the highest peak to the r.m.s. (root-mean-square) noise are calculated in each window. If the first ratio exceed a predefined threshold value, and if the second ratio also exceeds a preset (determine by trial and error) threshold value, the distance between these two peak is retained as valid. The spatial resolution increases by reducing the small window size and consequently increasing the number of vectors which would increase the accuracy of the process. Output of MPIV results is post processed by the function `mpiv_filter`. This function uses a small area of the image which includes  $3 \times 3$  to  $9 \times 9$  vectors to calculate the mean, median, standard deviation and the number of valid vectors in the area. These values are used to determine whether the vector in the area of interest is a valid vector or not. If the target vector is within the range of vector standard deviation from the mean or the median value, it is then considered as good vector. Otherwise, it is removed from the valid vectors.

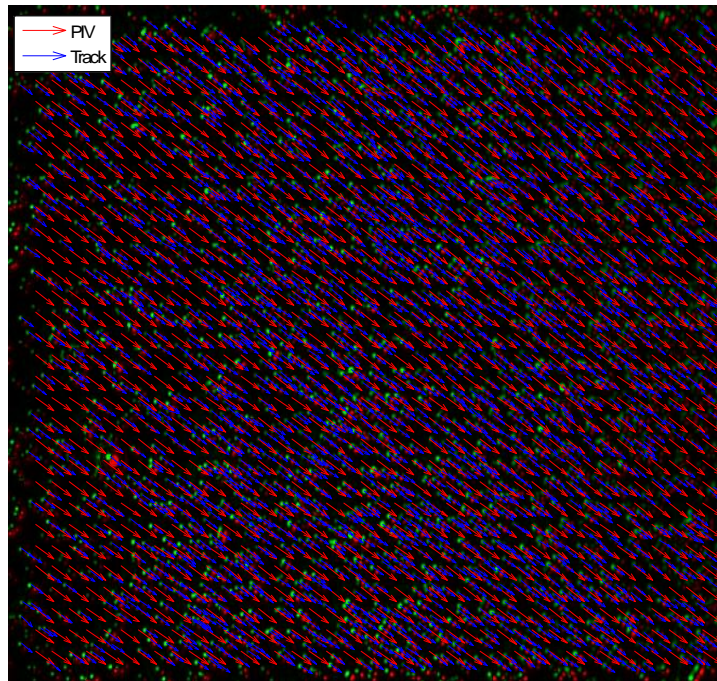
### **2.9.3 Limitations of particle tracking**

Having applied these methods to the optical flow images, an investigation was performed to determine which is more accurate and has fewer limitations. To address this question, displacements vectors were calculated by PIV as well as Particle Tracking and are shown in Figure 10. Although figure 10.A indicates similarity between the results (red vector represents PIV and blue vectors Track), Figure 10.B does not prove equality by representing the difference between the vectors lengths along x and y-directions. The scattered plot shows a non-zero difference corresponding to some beads, and zero difference for the others. The next step is to evaluate such beads and their intensity profiles as well as to determine the

method which does not work for these beads. As such, the beads found using MATLAB had an intensity profile as well as PIV-Track difference are indicated in Figure 11. Figure 11.A to D show that at such positions, beads are aggregated and hence have small distances with their closest neighbors. As pointed out in Section 2.9.1, Track tools do not track the beads whose displacements are greater than the mean inter particle separation; therefore, the aggregated beads are not tracked using this approach. Thus, Track gives zero displacements corresponding to the aggregated beads which cause the non-zero difference between Track and PIV. In figure 12, two isolated beads as well as their intensity profiles along x- and y-axis and the difference between PIV and Track measurements are indicated. Looking at their intensity peaks which are in general greater than those of aggregated beads, and PIV-Track differences, which are very small compared to those of aggregated beads, confirms that isolated beads are well tracked and hence PIV matches with Track. However, this is not true for the aggregated beads. Therefore, PIV which is able to find the movements of aggregated beads by not including the mean inter particle separation limitation, is used for the displacement determination

Figure 13 indicates the displacements calculated by PIV on the cell phase image. The vectors show the direction of traction force, into the cell. Most of the vectors are concentrated in the cell lamellipodia, and the cell nucleus is not involved in traction force.

(A)



(B)

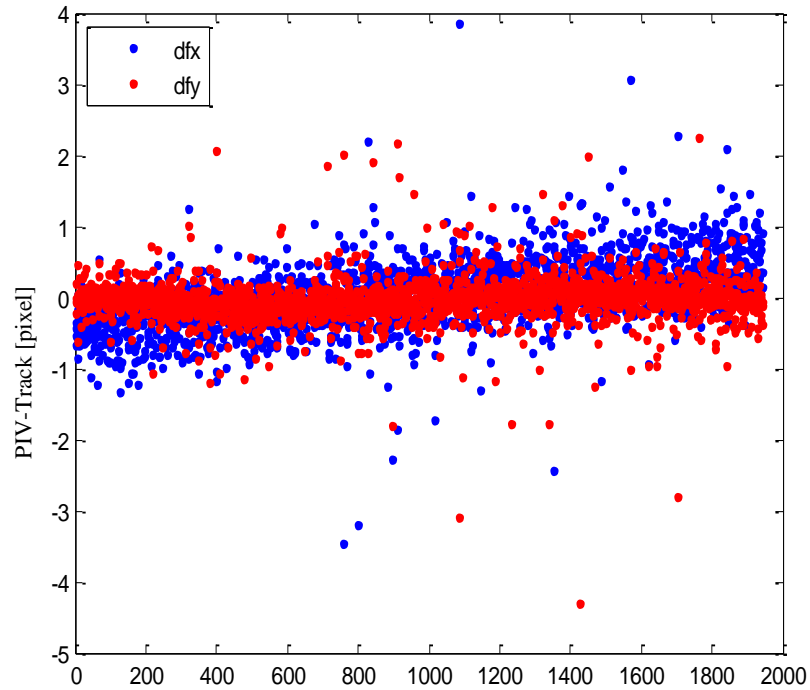
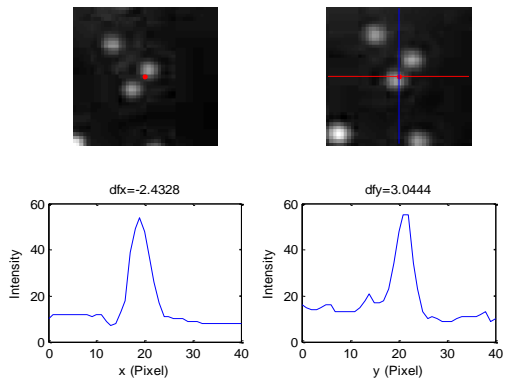
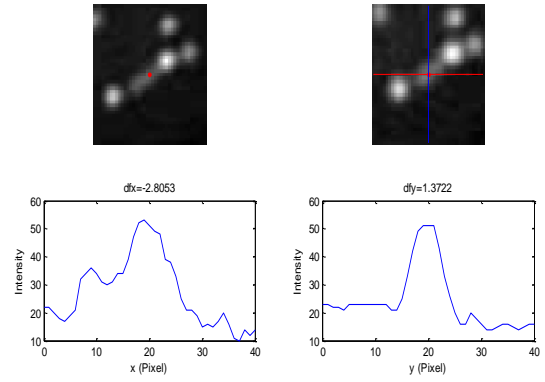


Figure 10. Comparison between PIV and Track. A) Red vectors PIV and blue vectors Track displacements. (B) Difference in pixel between PIV and Track along x- and y- axis

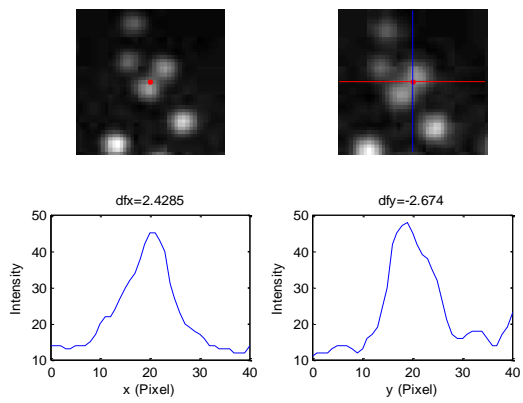
A



B



C



D

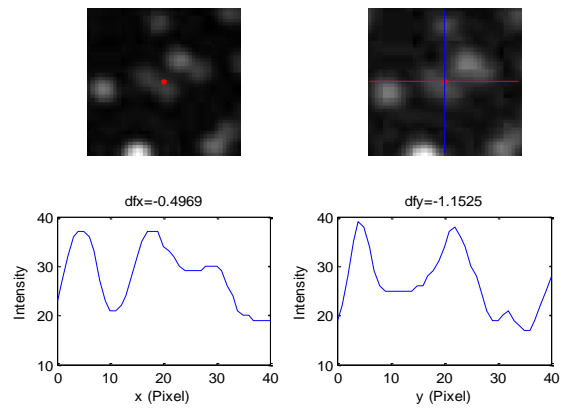
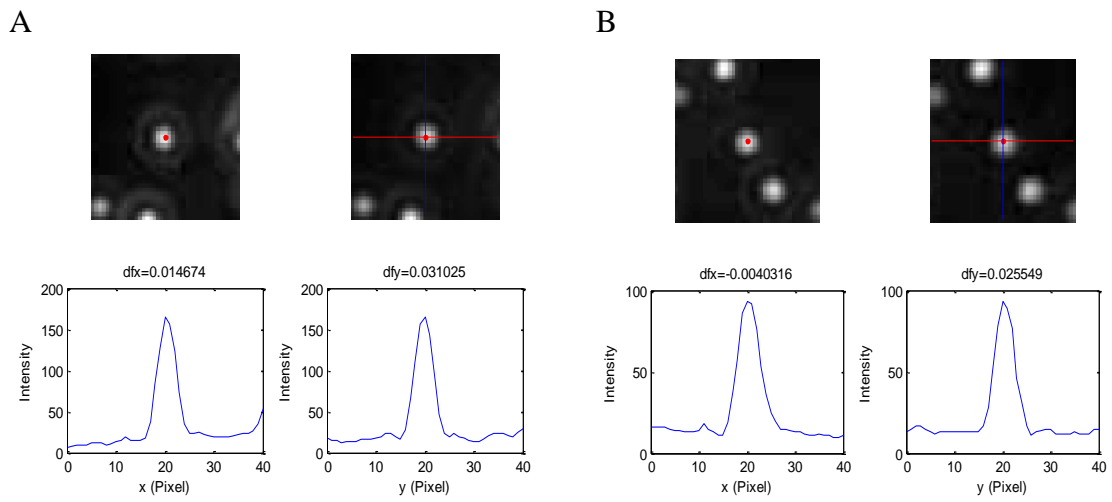
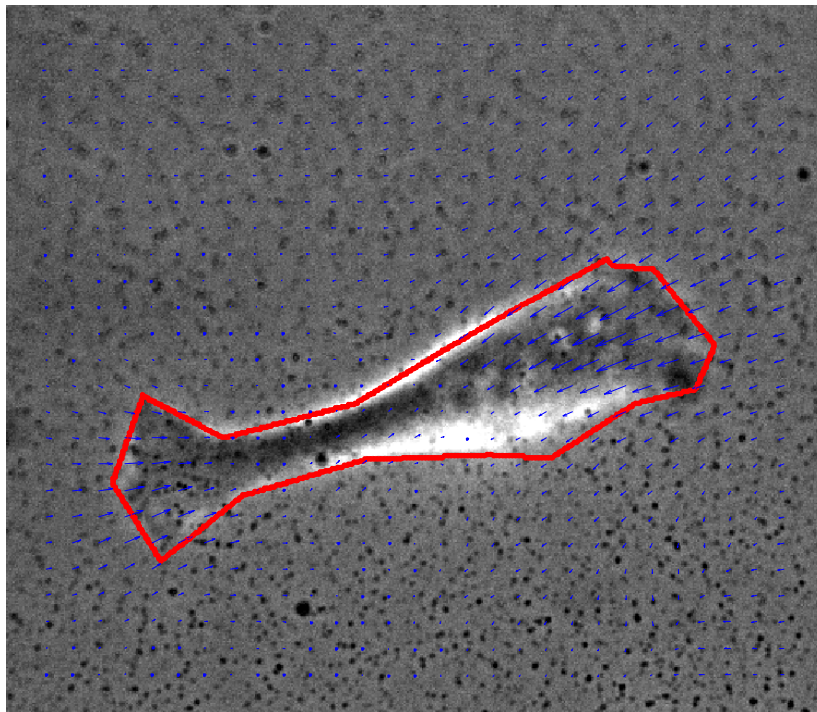


Figure 11. Aggregated beads and their intensity profile along x- and y- direction



**Figure 12. Isolated beads with their intensity profile along x and y direction**



**Figure 13. Displacement fields and cell boundary on the cell phase image**

## 2.10. Finite Element analysis in ANSYS

Once the substrate displacement fields are calculated, the next step is to find the stress that cells apply to the substrate. A 3-D finite element analysis (FEM) in ANSYS APDL (Parametric Design Language) was used to calculate the finite traction stresses due to the small movements of the beads on the substrate. Traction stresses were calculated using the displacement vectors, the gel image dimensions, fixed boundary condition at the bottom, the substrate Young's modulus and Poisson ratio as the inputs.

### 2.10.1. The 3-D model for substrate

Substrate was modeled as a rectangular volume or a brick with eight-nodes (Element type: Solid 185) in ANSYS. The length and width of this volume are equal to the image dimensions, and, the height is equivalent to the gel thickness. Thickness of the substrate was calculated by having the volume of acrylamide solution as well as the glass area. The cover slip glass dimension is  $25 \times 25 \text{ mm}^2$  and the solution volume added on it was  $64 \text{ }\mu\text{l}$ . Therefore, the height calculated to be about 100 microns. Hydrogel material properties are also required as the input for the model description. PA gel is a linear, isotropic and elastic hydrogel with Poisson ratio of 0.4. Young's modulus of the substrate is tunable by changing the concentration of Acrylamide and Bis-acrylamide in the gel solution as mentioned earlier. Gels were made with different stiffness ranging from 3.5 kPa to 20 kPa. The volume is then meshed using a finite element size. This size must be whether the same as the window size selected for PIV function or one of its factors. If the mesh size is bigger than the window size, a single mesh unit would include an area with several displacement vectors and this lowers the accuracy of analysis; nonetheless, a very small mesh size causes longer time ANSYS

analysis. The mesh size we selected was 16 pixels (2.6 micrometer) considering a 64 pixels (10.6 micrometer) PIV window size.

### 2.10.2. Determining nodal traction stresses

The first step in FEM analysis was to build a model with the gel characteristics described earlier. To perform the FEM analysis and calculate the traction force, one can always use ANSYS GUI (graphic user interface); this is not convenient for our analysis due to having a large number of nodes. Therefore, we made scripts which included command lines to make the model and apply the load on it. A fixed boundary condition was applied to the bottom of substrate. Additionally, nodes outside the cell boundary were assigned zero external forces. While on the nodes inside the cell boundary the nodal displacements derived from MATLAB analysis were applied. The problem was then solved in ANSYS using a structural analysis. The results of this solution were imported from the text files that ANSYS provides from the results. These files include the location of nodes on the gel top and their resultant stress values.

Since the elastic substrate is in equilibrium condition, the following equation is applied,

$$[K]\{u\} = \{F\} \quad (2.3)$$

Where  $[K]$  is the global stiffness matrix,  $\{u\}$  the nodal displacement vector, and  $\{F\}$  is the nodal force vector. The equilibrium condition can further be written in terms of sub-matrices and sub-vectors as

$$\begin{Bmatrix} [k_{cc}] & [k_{cs}] \\ [k_{cs}]^T & [k_{ss}] \end{Bmatrix} \begin{Bmatrix} \{u_c\} \\ \{u_s\} \end{Bmatrix} = \begin{Bmatrix} \{F_c\} \\ \{F_s\} \end{Bmatrix} \quad (2.4)$$

Where s subscript denotes the degrees-of-freedom (DOFs) where displacements are known; and c subscript denotes the rest of DOFs where the forces are known. For nodes outside the cell boundary, their nodal forces are zero. Using this information the above equation becomes

$$\begin{Bmatrix} [k_{cc}] & [k_{cs}] \\ [k_{cs}]^T & [k_{ss}] \end{Bmatrix} \begin{Bmatrix} \{u_c\} \\ \{u_s\} \end{Bmatrix} = \begin{Bmatrix} \{0\} \\ \{F_s\} \end{Bmatrix} \quad (2.5)$$

Equation (2.3) is the key equation that is used to find the traction forces exerted by the cells having the nodal displacements as well as the gel stiffness.

### 2.11. Post-processing

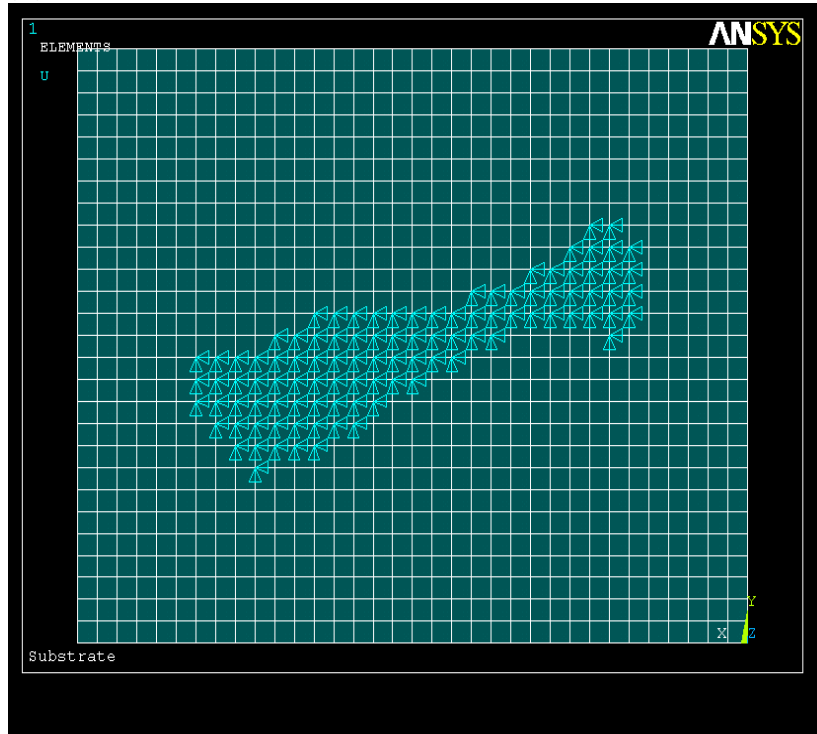
Text files that include the nodal shear stress were exported from ANSYS. Having the nodal shear stress and each element area, the nodal traction force as well as the total traction force was calculated. Figure 14 shows how the model looks like in ANSYS, indicating the meshed rectangular volume and the displacements applied on the top. Figure 14 A is the top view and 2.7 B is the isometric view. The cell is placed on the top of the model on the x-y plane. Therefore, the elements of shear stress required to calculate the nodal shear values are  $S_{xz}$  and  $S_{yz}$ . The stress at each node is then calculated by:

$$S_i = \sqrt{S_{i_{xz}}^2 + S_{i_{yz}}^2} \quad , \quad F_i = S_i \times da \quad (2.6)$$

Where I, is the node index (number) and da, is the element area.

$$S_{Total} = \sum_{i=1}^n S_i \quad , \quad F_{Total} = \sum_{i=1}^n F_i \quad (2.7)$$

(A)



(B)

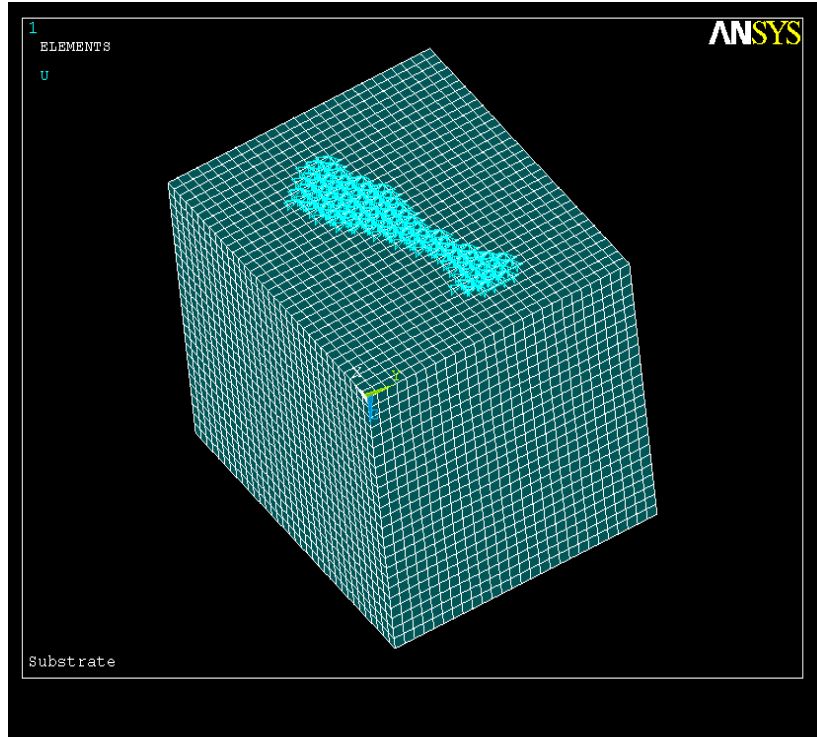


Figure 14. Gel rectangular volume model in ANSYS with the cell (A) Top view, (B) Isometric view

Having the nodal stress values, a stress map or stress distribution is plotted in Figure 15 with the cell boundary. The color bar next to the figure shows the stress intensity. Larger stress values are observed at the cell lamellipodia, corresponding with the greater vectors on these sites, and smaller stresses are around the cell nucleus as well as on outside the cell boundary.

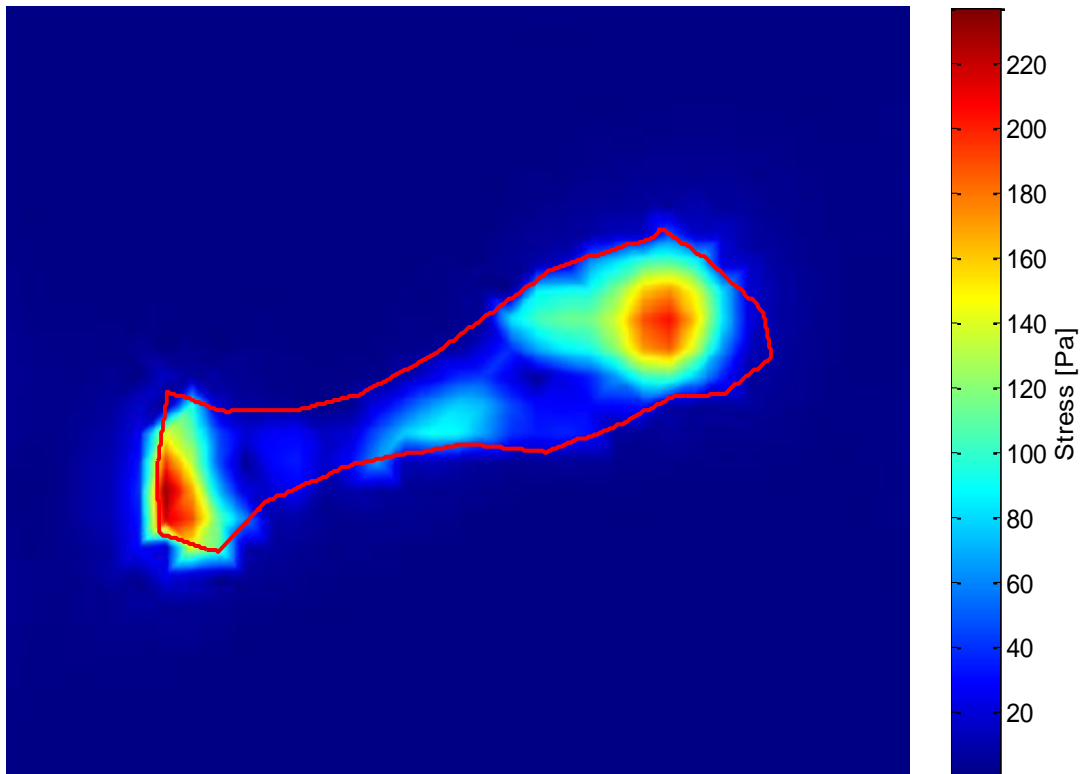


Figure 15. Stress distribution with the cell boundary

## 2.12. Validity of ANSYS model

The ANSYS model was validated through the following analyses. These analyses were performed based on the Elasticity principles for a hydrogel. Shear stress and shear strain behaviour were evaluated in the elastic rectangular model designed in ANSYS. The results were compared to the theoretical predictions to determine the validity of the model.

Shear stress, denoted by  $\tau$  is the stress component parallel to the cross section. Normal stress, on the other hand arises from the perpendicular component to the cross section. Contractile cells apply tensile stress on the substrate and generate shear stress. Stress is defined as the force divided by the area it is applied on ( $\tau = \frac{F}{A}$ ). Relation between the shear stress and strain is given by

$$\tau = \gamma G \quad (2.8)$$

Where  $\gamma = \frac{\Delta l}{l}$ ,  $G = \frac{E}{2(1+\nu)}$ , E is the Young's modulus and  $\nu$  is the Poisson's ratio.  $\Delta l$  is the strain and l is the gel height.

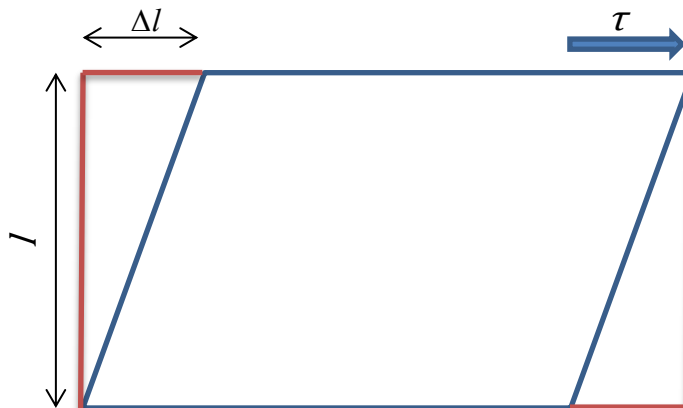


Figure 16. Shear stress and shear stain

In Eq. 2.8,  $\gamma$  represents the strain and  $\tau$  the stress. For a linear elastic substrate  $\gamma$  is a constant value and is expressed as the ratio of total deformation to the initial height of the elastic body in which the forces are being applied. Therefore, when going down into the gel or along the cross sections below the surface on which the loads are applied (decreasing  $l$  in Figure 17), total deformation has to be decreased in a linear manner correspondingly to keep strain a constant value. Additionally, the total shear stress that is transmitted to the bottom layers remains the same. Using this concept to test the validity of FEM method and the meshed model uniform nodal loads were applied on the top and then the problem was solved to acquire the total deformation as well as the total stress on the underlying cross sections. The results of this analysis are predicted in Figure 18 which shows the total deformation on five cross sectional layers of the gel from the top, where the load is applied. The total stress on the same layer was also calculated. Total shear stress is the same on these layers which matches with the theory. The linear decrease of the deformation in Eq. 2.9 and the constant total shear stress show that our FEM analysis works well since it matches with the theories.

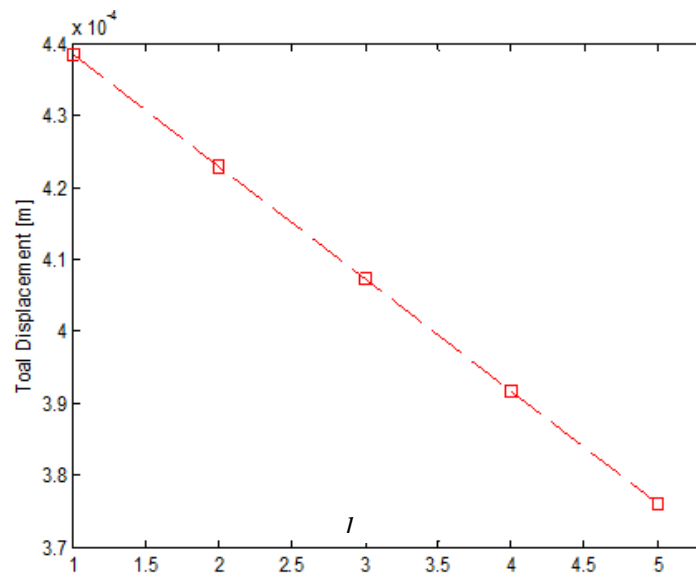


Figure 17. Total displacement on five cross sections of the gel when nodal uniform displacements (2 microns) were applied on the top

### 2.13. Traction stress dependency on gel thickness

As mentioned earlier, gel thickness used in the 3-D model approximated the actual gel thickness ( $\sim 100 \mu\text{m}$ ) used in the experiment. Cells cultured on the gel with higher stiffness were seen to be larger compared to those on the soft gel. The dimension of cropped images were seen to be larger compared to those on the soft gel. The dimension of cropped images changed from  $\sim 300 \times 300 \text{ pixel}^2$  for cells with a smaller area on the gel to  $\sim 600 \times 600 \text{ pixel}^2$  for cells with larger area. So a different gel thickness could change the result. To verify this, gel length and width were kept constant and the height was changed from a hundred pixels ( $16 \mu\text{m}$ ) to 800 pixels ( $133 \mu\text{m}$ ). Total stress was then calculated for different thicknesses. The results, presented in Figure 18 imply that by increasing the gel thickness or the gel height in the model, total stress on the gel surface decreases; nonetheless, the effect plateaus at  $\sim 400$  pixels. Thus, in order to save the time in the FEM analysis and since the total stress remains constant for thickness above 400 pixels, we assign gel height equal to 60 microns for cells with relevantly smaller size and, a hundred  $\mu\text{m}$  for those with bigger spreading area.

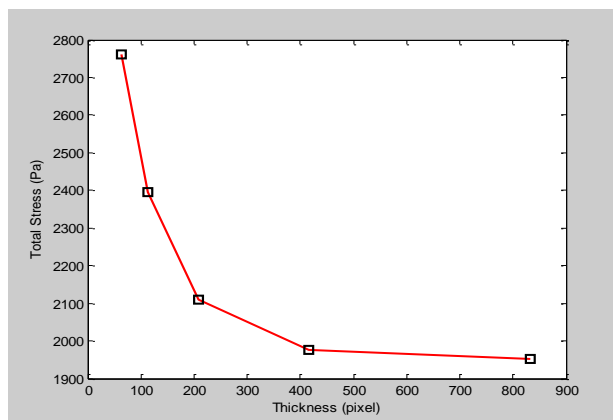


Figure 18. Total Stress change as a function of gel thickness

## 3. Results

### 3.1. Comparison of traditional method with the current method

In order to show the difference between the new approach of coating the beads on the gel top and the traditional methods of embedding the beads in the gel, a PA gel with 7.5 kPa Young's modulus was made and mixed with the green fluorescent beads. Then the gel was coated with the red beads on the top using the new method described in Section 2.2. Thus, the green beads are in the gel and the red are on the top. Cells were cultured on the gel. Red and green fluorescent filters were used in CTF microscopy to acquire separate images of optical flows for green and red beads. Traction force due to the displacement of red beads was measured for three cells and the results were compared with the traction force generated from the green beads displacements. This comparison is indicated in table 3. Additionally, comparison of traditional method with the new method was performed through simulation via replacing the displacements of the first layer with the displacements of the nodes randomly picked from the second layer in the gel. CTF was calculated for the same cells. The simulation column in Table 3 belongs to this result. The values are the average of 10 runs. The last two columns show the ratio of traction force generated by the movement of green beads to the red beads well as the ratio of simulation to the red beads experiment. These values indicate that if the beads are embedded within the gel (traditional method), traction force would be about 10 to 20% less than the traction force generated by the beads embedded on the top (novel method). This means that there is about 20% difference between the previous methods and our method. The last column also confirms this conclusion. These results suggest that our method is more accurate compared to the other existing methods. Also this difference shows the importance of evaluating the effect of out of focus beads. In the

section 3.3 we will show that even by coating the beads on the top limiting the beads completely on the top layer is impossible. Some beads go into the gel and hence decrease the result's accuracy. Therefore, the next step is to calculate the traction forces and then investigate the effect of out of focus beads.

**Table 2. Comparison of traditional method by the novel method using experiments and simulation CTF from red and green bead (experiment) and from simulation by replacing the second layer displacements from inside the cell on the top layer for three cells on 7.5 kPa gel**

Cell	CTF- Red [nN] New method	CTF-Green [nN] Traditional method	Simulation [nN]	CTF- (Green/Red)%	CTF- (Sim./Red)%
1	18	16	13	89	70
2	9	7	7	80	78
3	44	36	35	83	79

### 3.2. CTF analysis results

Traction forces of individual contractile cells on the substrate were measured using the new approach. PA gels were coated with different ligands, fibronectin and collagen. Cells were seeded on the gels with Young's modulus of 3.5, 7.5, and 20 kPa were left to adhere to the underlying matrix. For each gel condition (stiffness) between 10 and 15 healthy cells were found and selected for imaging. Images were then analyzed and traction force that each cell generated on the substrate was calculated using FEM analysis in ANSYS. The average cell traction force was then calculated for the cells on the same gel stiffness, and on different ligand types (collagen, fibronectin). The average traction force as

a function of gel stiffness is indicated in Figure 20 and Table 3. Error bars representing the standard deviation.

When adhered to the substrate, not only fibroblasts apply force on the underlying substrate, but also they spread and change their adherent area. Fibroblasts are in various shapes and sizes; some of them were seen to have fan-like shapes, some were spindle-like, and the others looked like triangles, often include a larger area compared to those of spindle-like cells. Based on this observation, we assumed that fibroblast shape and area engage a relationship with CTF, as different cell shape and area were found to have different CTF values. In addition, studies on investigating the relation between cell shape and CTF were focused on determining which of these variables the significant predictor of the others is [38-40]. Therefore, in addition to the traction forces, cells spreading areas were measured and the average cell areas as a function of gel stiffness are shown in Figure 20.B.

Figure 20.A and B show that the average CTF and the average cell area increase as the substrate stiffness increases for cells grown on collagen as well as on fibronectin. This result suggests that cells on the soft gels apply smaller traction forces and spread smaller areas, whereas, on the stiffer substrate they spread more and apply greater forces. In addition, the difference between collagen and fibronectin values indicates that cell responses depend on ECM ligands type. It seems that cells on fibronectin exert greater forces compared to the cells grown on collagen ligand. Previous studies on cell responses to the mechanical stimuli also indicate that cells responses change on substrate with different stiffness. Studies on A7 and M2 melanoma cells indicate that cells change their stiffness in order to match with that of their substrate [41-43]. They also indicate that cells responses depend on the type of ECM

ligands. Our results show that CTF changes as a function of gel stiffness. These results agree with the previous studies on cellular responses and prove that our measurement method is valid.

Figure 21 shows the relation between cell area and CTF for cells grown on fibronectin and on collagen gel with different stiffness. Each point corresponds to the CTF and the area of one cell. The result suggests that CTF and the cell area are directly proportional since the larger the cell area, the greater the traction force is. However, it is not certain which cell area or cell traction force is determinant from the other.

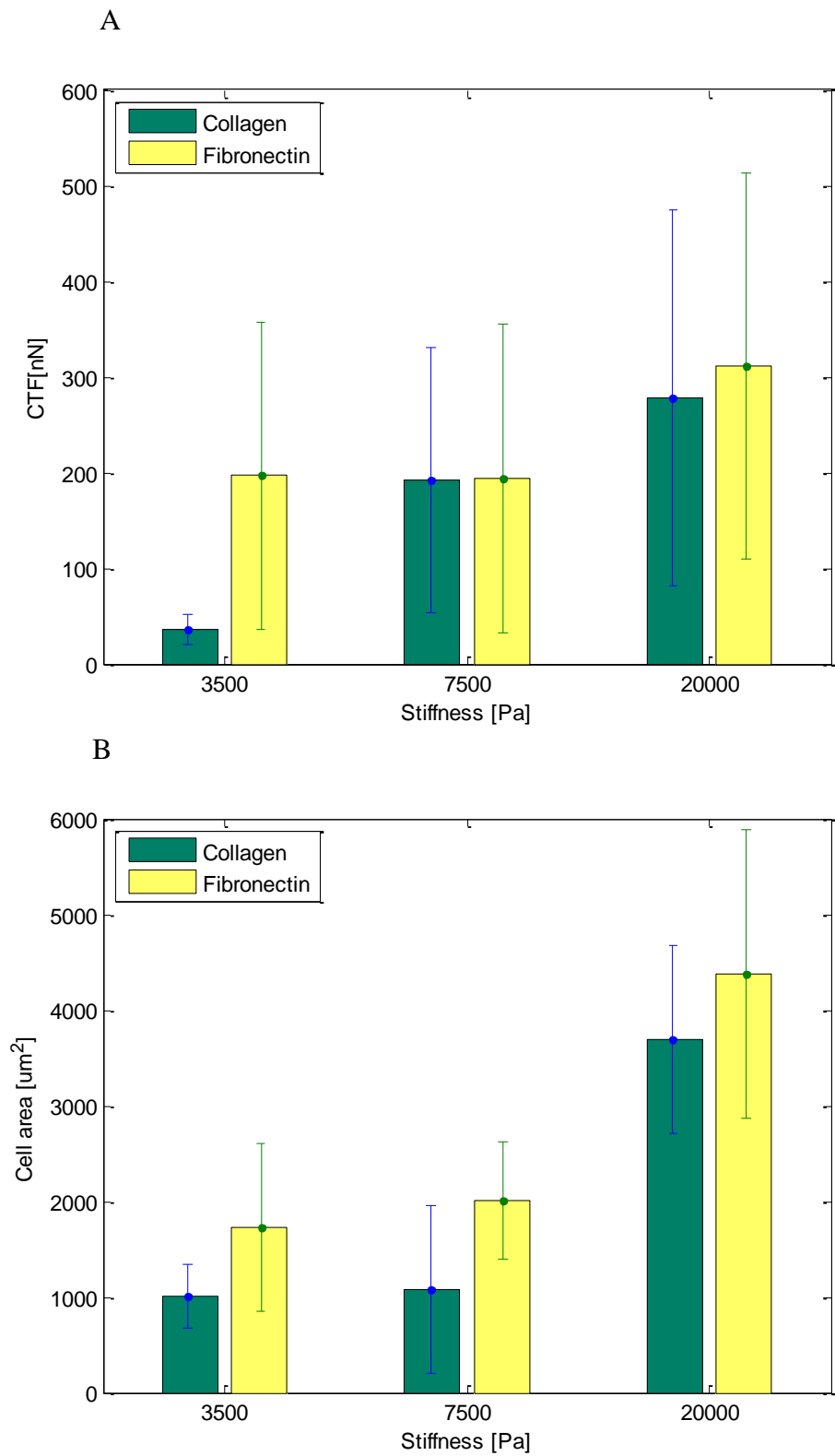


**Figure 19. CTF and Cell area as a function of stiffness A) CTF [nN] B) Cell area [μm<sup>2</sup>]**

**Table 3. Average CTF and average area of the cells grown on fibronectin as well as on collagen on gel with stiffness 3.5, 7.5 and 20 kPa**

<b>Fibronectin – number of cells &gt;10</b>				
<b>Young's modulus [kPa]</b>	<b>Average CTF [nN]</b>	<b>STD</b>	<b>Average Area[<math>\mu\text{m}^2</math>]</b>	<b>STD</b>
<b>3.5</b>	197	160	1727	943
<b>7.5</b>	194	162	2002	615
<b>20</b>	312	203	4380	1512
<b>Collagen - number of cells &gt;10</b>				
<b>3.5</b>	35	16	1009	327
<b>7.5</b>	192	139	2094	874
<b>20</b>	278	197	3698	987

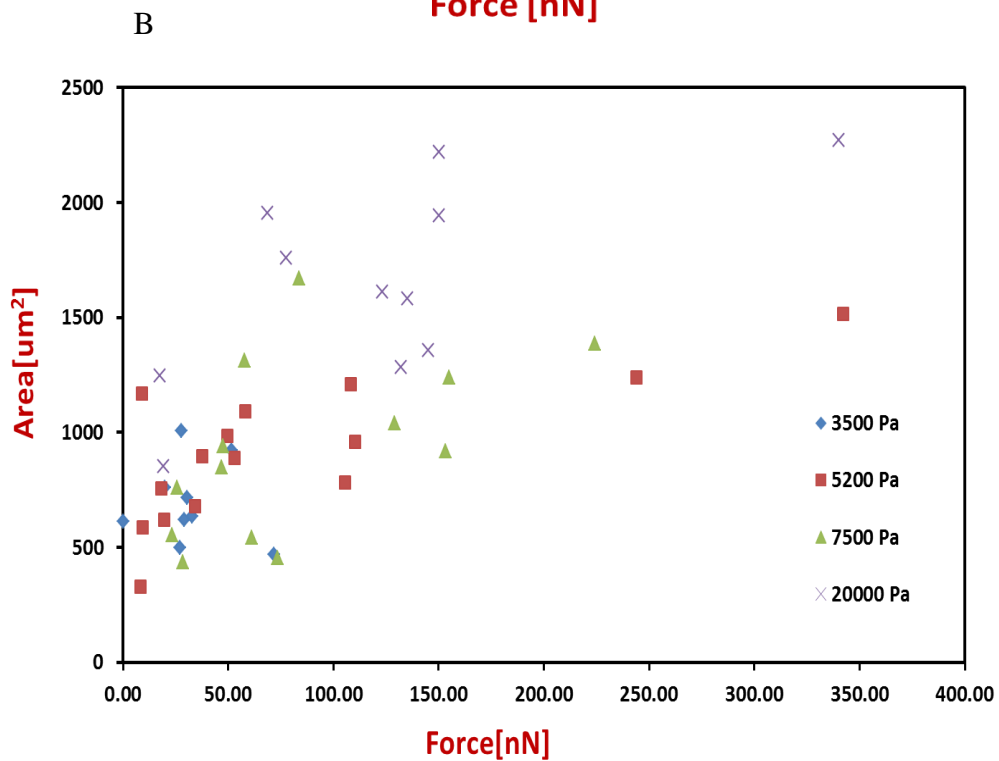
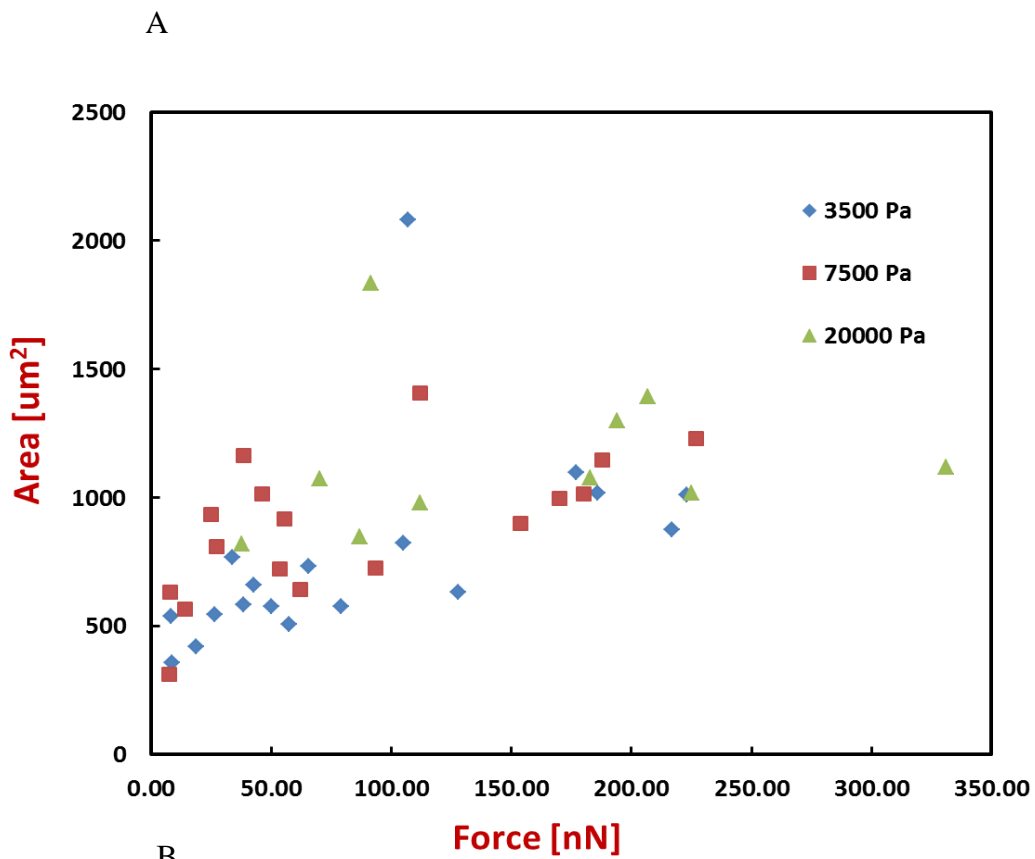


Figure 20. Cell area as a function of CTF for A) Fibronectin and B) Collagen.

### 3.3. Evaluating the effect of out-of-focus fluorescent beads

As mentioned earlier, fluorescent markers are required to track the small drifts on the substrate generated from the cell traction force. Fluorescent beads with a diameter of  $0.2\ \mu\text{m}$  were used for this purpose. Due to their size, some of the beads will fall down and penetrate into the gel after they are coated on the top. When taking the images, the microscope objective is focused on the gel top. Therefore, the beads which remain on the top are in focus and those piercing in the gel are out of focus. The effect of out of focus beads is important, because they introduce uncertainty in CTF measurements as pointed out in Section 3.1. Therefore, experiments and analysis were performed to show the beads distribution in the gel as well as evaluating their effect on the CTF measurement results. First, a PA gel was made and coated with green beads with smaller diameter on the top using the novel method explained in Section 2.2. Other green beads with greater diameter ( $2\ \mu\text{m}$ ) were also prepared and dropped on the gel. Big beads are used to show the gel top since they are not small enough to go into the gel and will remain on the surface. Then a confocal Zeiss microscope was used to acquire images from the gel cross sections by focusing the objective on different planes along the gel height. The z-stack includes about  $40$  to  $50\ \mu\text{m}$  of the gel from the top and the distance between the cross sections is  $50\ \text{nm}$ . The images are then analyzed using a 3-D particle tracking MATLAB toolbox. The packages “bpass3d” and “pkfnd3d” were used to spatially filter the images and remove the noise and to find the positions of beads on each layer. Figure 22 shows the number of out of focused beads as a function of distance from the gel top. The smaller peak corresponds to the density of big beads that are on the surface, whereas the larger peak indicates where the majority of small beads are laced. Most of the small beads are distributed on the top layer. Small population of beads is on floating in the

HEPES buffer solution above the gel. These beads represent the distance between 56 to 60  $\mu\text{m}$  in the graph. The bead density decreases as going down in the gel (to the 0 on x-axis) and tends to zero for the lower layers. This graph is the evidence for our assumption regarding the presence of a small percentage of the fluorescent markers inside the gel and that how this density decreases as a function of distance from the top.

The advantage of coating the beads on the surface is that the percentage of out of focus beads to the overall bead number is small. Our method, therefore, can measure the traction force more accurately. On contrary, in traditional methods the bead solution is mixed with the gel and hence, the percentage of out of focus beads to the total beads number would be greater.

Displacements of the nodes on the top layer were replaced with the displacements of the second layer acquired from ANSYS. The second layer displacements correspond to the beads movements in the gel which are at a distance equal to the mesh size from the top. CTF was then calculated and compared with the CTF at the top. The results are indicated in Figure 22.

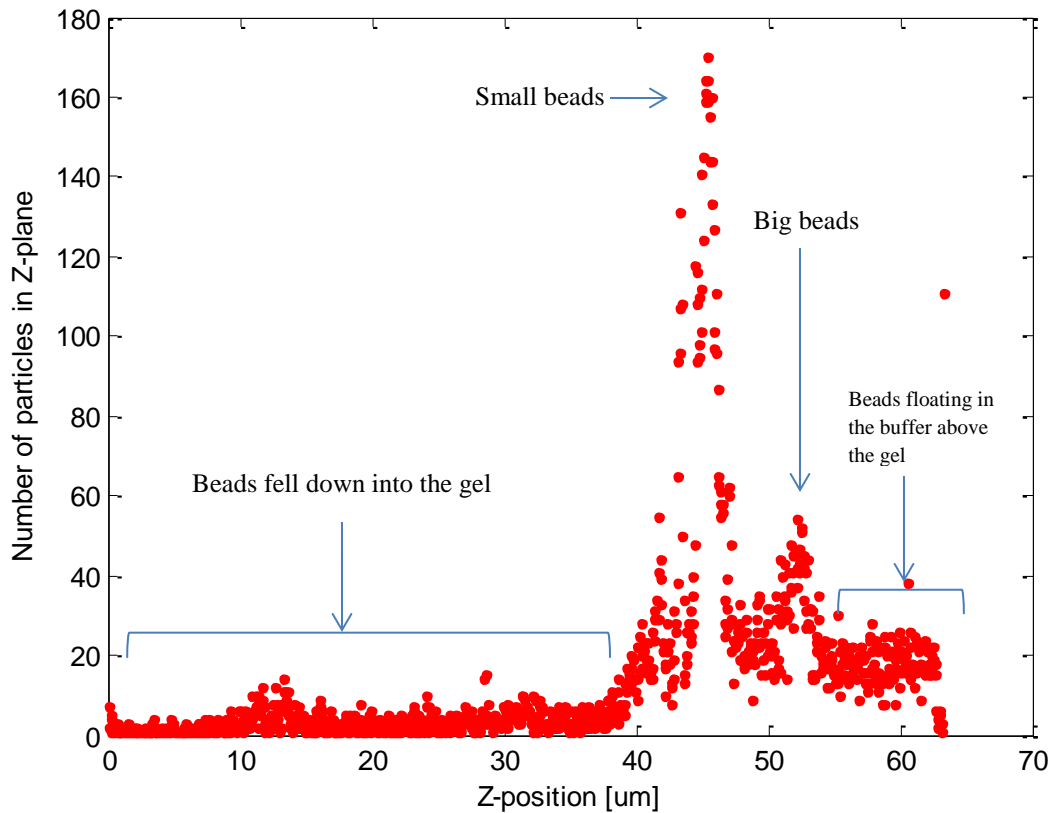
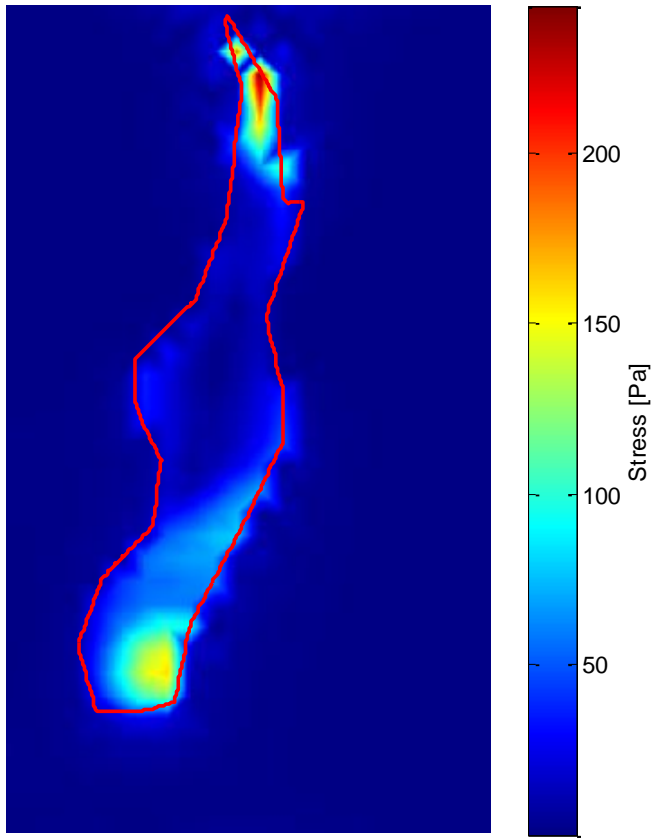


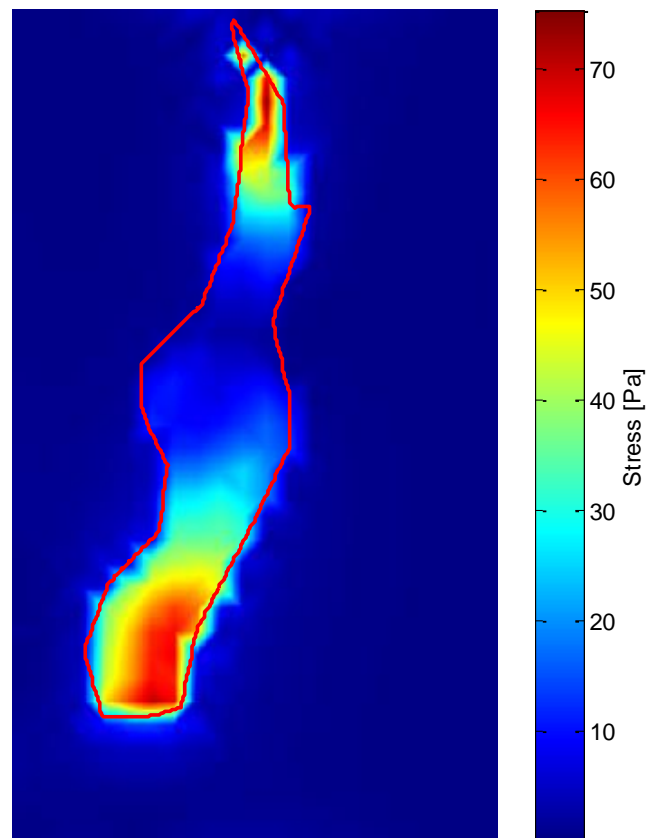
**Figure 21.** Density of fluorescent beads (out of focus) as a function of distance from the top in the gel. Y-axis the number of beads in distance  $z$  from the gel top. Zero corresponds to 60 micron (~1000 pixels) below the gel surface. The smaller peak represents the large beads on the top and the largest peak indicates where the majority of small beads are placed.

To measure the effect of out-of-focus beads, the displacements on the top were replaced with the displacements on the second layer which represent the displacements of beads out-of-focus. Traction stresses were then calculated. The stress distribution in the Figure 23 shows the decrease in the tractional stress due to replacing the first layer displacements on the top with those of the second layer. This result as well as Figure 22 indicates that the effect of out-of-focus beads decreases on the deeper layers in the gel. As such, the CTF decreases (28.7nN for the second layer and 64nN for the top layer).

A



B



CTF= 46 nN

CTF= 29 nN

Figure 22. Stress distribution and traction force, replacing the displacement fields of the second layer on the top. (A) The load applied on the top, (B) when the load is replaced by the displacements of the second layer.

## Conclusion and Future Works

Various methods have been developed to measure the CTFs by applying traction force microscopy for a continuous hydrogel. Although these methods have advantages compared to other method of CTF measurements, they represents some limitations that results in the measurement uncertainty. In order to overcome these limitations, we developed a new approach in CTFM method. In our novel approach, fluorescent beads were coated to the top of a hydrogel, while in the previous methods beads were embedded in the gel. This improvement enhances the accuracy of CTF measurement results.

Additionally, the other disadvantage of some of the existing methods was using an infinite half space approximation for the substrate with finite thickness which introduced errors. To overcome this problem, we applied a 3-D FEM analysis in ANSYS in order to take the finite thickness of the substrate into account. CTFs were then measured using the new method for cells grown on PA gel with different stiffness and coated with different types of ligand. The result of CTF measurement using the new technic was compared with CTF using the traditional techniques which indicated ~20% difference between these methods. This shows that traditional method is underestimating the CTF results (Table 3). As mentioned above, the effect of out of focus beads were then evaluated both experimentally and analytically (Figure 21 and 22). These results indicated that out of focus beads effect is considerable, and hence, developing methods that can control and decrease this effect, would increase the accuracy of the CTF measurements, which is a part of our future work.

## 4. Appendices

### 4.1. Appendix I- Pre-processing and post processing MATLAB codes

#### 4.1.1. Pre-processing

```
%% Defining variables/constant
```

```
foldn='folder name'
```

```
Dishn='Dish number'
```

```
posn='Cell position'
```

```
scal1=1e-6/6; scal2=1/6;
```

```
% % Reading the images
```

```
a1=imread ([Dishn,'_wMedium_',posn,'_Fluor.TIF']);
```

```
a2=imread ([Dishn,'_wTrypsin_',posn,'_Fluor.TIF']);
```

```
a3=imread ([Dishn,'_wMedium_',posn,'_Phase.TIF']);
```

```
%% Making RGB image from the gray scale images
```

```
cimg(:,:,3)=zeros(size(a2));
```

```
cimg(:,:,1)=double(a2)/(max(double(a2(:))));
```

```
cimg(:,:,2)=double(a1)/(max(double(a1(:))));
```

```
imshow (cimg,[]);
```

```

%% Drift removing

for i=1:4

[xd(i) yd(i)]=im_shift(a1,a2);

Xd = mean (xd(i));

yd = mean(yd(i));

end

imshow (a3,[]);

rg2=round (getrect);

rg2(3)=[round(rg2(3)/16)]*16; rg2(4)=[round(rg2(4)/16)]*16;

imgf_a1=imcrop (a1,rg2);

imshow (imgf_a1);

figname=[Dishn,posn,'_wMedium.tif'];

imwrite (imgf_a1,figname);

figure(2),imgf_a2=imcrop(a2,[rg2(1)+xd rg2(2)+yd rg2(3) rg2(4)]);

imshow (imgf_a2);

figname=[Dishn,posn,'_wtrypsin.tif'];

imwrite (imgf_a2,figname);

%% Image cropping

imgf_a3=imcrop (a3,rg2);

imshow (imgf_a3);

figname=[Dishn,posn,'_phase.tif'];

```

```

imwrite(imgf_a3,filename);

close all;

cimg2 (:,:,3)=zeros(size(imgf_a2));

tempr = double(imgf_a2)/(max(double(imgf_a2(:))));

tempg = double(imgf_a1)/(max(double(imgf_a1(:))));

cimg2 (:, :, 1) = tempr-tempg;

cimg2 (:, :, 2) = tempg-tempr;

figure,imshow(cimg2,[]);

```

**%% Using PIV for for displacement calculations**

```

[xi, yi, iu, iv, D] = mpiv(imgf_a2,imgf_a1,64,64,0.5,0.5,25,25,1,'mqd',2,0);

[iu_f,iv_f,iu_i, iv_i] = mpiv_filter(iu,iv, 2, 2.0, 3, 0);

[iu_s, iv_s] = mpiv_smooth(iu_i, iv_i, 1);

[xm, ym] =meshgrid([min(xi):xi(2)-xi(1):max(xi)],[min(yi):mean(diff(yi)):max(yi)]);

figure(4), imshow(cimg2,[]);

hold on, quiver(xm',ym',iu_s,iv_s,'b');

filename=[Dishn,posn,'.tif'];

imwrite (cimg2,filename);

xs1=xm'*scal1;

ys1=ym'*scal1;

dx2=iu_s*scal1;

dy2=iv_s*scal1;

```

```
%% Drawing the cell edge
```

```
Figure (5), imshow(imgf_a3,[])
```

```
[bw,xc,yc]=roipoly;
```

```
reg = bwlabel(bw);
```

```
[s,l]=bwboundaries(bw);
```

```
g=regionprops(l,'PixelList');
```

```
hold on,plot(s{1}(:,2),s{1}(:,1),'r')
```

```
hold off
```

```
imshow (cimg2,[]);
```

```
hold on, quiver (xm', ym', iu_s, iv_s,'b');
```

```
plot(s{1}(:,2),s{1}(:,1),'r')
```

```
hold off
```

```
Cell_area=bwarea(bw)*(scal2^2);
```

```
% Saving displacements and position list files for ANSYS
```

```
fid= fopen([Dishn,posn,'_cell_crop4.txt'],'w');
```

```
fprintf(fid,'%10.4e \t %10.4e\n',[s{1}(:,2)*scal1 s{1}(:,1)*scal1]);
```

```
fclose(fid);
```

```
save([Dishn,posn,'_disp.mat'],'xs1','ys1','dx2','dy2','rg2','Cell_area');
```

### 4.1.2. Post-processing

```
%% Defining variables/constant
```

```
Dishn='Dish number'
```

```
posn='Cell position'
```

```
load([Dishn,posn,'_disp.mat']);
```

```
scal1=1e-6/4; scal2=1/4;
```

```
length = rg2(:,3)*scal1;
```

```
width = rg2(:,4)*scal1;
```

```
height = 400*scal1;
```

```
meshsize = 16*scal1;
```

```
%% Making ANSYS script for model definition
```

```
Filn = [Dishn,posn,c '.txt'];
```

```
fid = fopen(filn,'w');
```

```
line1 = ['/TITLE,newgel\n','/PREP7\n'];
```

```
fprintf (fid,line1);
```

```
line2 = ['ET, 1, SOLID185\n'];
```

```
fprintf (fid,line2);
```

```
line3=['KEYOPT,1,2,0\n','KEYOPT,1,3,0\n','KEYOPT,1,6,0\n'];
```

```
fprintf (fid,line3);
```

```
line4 = ['MPTEMP, \n','MPTEMP,1,0
```

```
\n','MPDATA,EX,1,,7500\n','MPDATA,PRXY,1,,0.4\n','!* \n'];
```

```
fprintf (fid,line4);
```

```

line5=['BLC4,0,0,',num2str(length),',',num2str(width),',',num2str(height),'\n'];
fprintf (fid,line5);

line6=['AESIZE,ALL,',num2str(meshsize),'\n','MSHKEY,0\n','MSHAPE,1,3d
\n','CM,_Y,VOLU \n','VSEL, , ,
\n','CM,_Y1,VOLU\n','CHKMSH,"VOLU"\n','CMSEL,S,_Y\n'];

fprintf (fid,line6);

line7 = ['MSHAPE, 0, 3d \n','MSHKEY,1\n','VMESH,_Y1\n','MSHKEY,0\n'];
fprintf (fid,line7);

fclose (fid);

pause;

```

**% % Determining positions and their corresponding displacements**

```

m=readnode ('NLIST.lis',2,2,20,7);

nlist = m.nodes;

xn = nlist(:,2); yn=nlist(:,3);

dxn = interp2(xsl',ysl',dx2',xn,yn);

dyn =I nterp2(xsl',ysl',dy2',xn,yn);

```

**%% Loading cell boundary**

```

celllist=dlmread([Dishn,posn,'_cell_',c,'.txt']);

xcell=(celllist(:,1));

ycell=(celllist(:,2));

Incell=inpolygon (xn, yn,xcell, ycell);

```

```
index_cell=find (Incell==1);  
  
xpos=xn(index_cell); ypos=yn(index_cell);  
  
xdisp=dxn(index_cell);ydisp=dyn(index_cell);
```

```
%% Making tables of load for ANSYS
```

```
B = [[1: size (index_cell, 1)]' (nlist (index_cell, 1)) xpos ypos xdisp ydisp];  
  
B(2:size(xpos,1)+1,:)=B(1:size(xpos,1),:);  
  
B (1,:)= [0:5];  
  
format shortG;  
  
dlmwrite ('table1.txt',B, '\t');
```

```
index_outcell= find (Incell==0);  
  
xout = xn(index_outcell); yout=yn(index_outcell);  
  
dxout = dxn(index_outcell); dyout=dyn(index_outcell);  
  
C = [(1: size (index_outcell, 1))' (nlist(index_outcell,1)) xout yout dxout dyout];  
  
C(2:size(xout,1)+1,:)=C(1:size(xout,1),:);  
  
C (1,:)= [0:5];  
  
format shortG;  
  
dlmwrite('table2.txt',C, '\t');
```

```
% % Making ANSYS script to apply the load on top
```

```
filn='ansys.txt';  
  
fid=fopen(filn, 'w');
```

```

line1=['*dim,Txy,table,',num2str(size(index_cell,1)),',5,1\n'];
fprintf (fid,line1);

line2 = ['*tread,Txy,"table1.txt"\n'];
fprintf (fid,line2);

line3=['*do,i,1,',num2str(size(index_cell,1)),',1\n'];
fprintf (fid,line3);

line4 = ['d,Txy(i,1),ux,Txy(i,4)\n'];
fprintf (fid,line4);

line5 = ['d,Txy(i,1),uy,Txy(i,5)\n'];
fprintf (fid,line5);

line6 = ['*enddo\n'];
fprintf (fid,line6);

line8=['*dim,loadf,table,',num2str(size(index_outcell,1)),',5,1\n'];
fprintf (fid,line8);

line9 = ['*tread,loadf,"table2.txt"\n'];
fprintf (fid,line9);

line10=['*do,j,1,',num2str(size(index_outcell,1)),',1\n'];
fprintf (fid,line10);

line11=['f,loadf(j,1),fx,0\n','f,loadf(j,1),fy,0\n','f,loadf(j,1),fz,0\n','*enddo\n','da,2,ux,0\n',
'da,2,uy,0\n','da,2,uz,0\n'];
fprintf (fid,line11);

fclose (fid);

pause;

```

```

%% Reading ANSYS output by “readnode” function

ress1=readnode('PRNSOL_', 'Dishn', 'posn', '.lis', 2, 9, 37, 7);

list_1=ress1.nodes;

% % Stress calculation

syz_1=list_1(:, 6); sxz_1=list_1(:, 7);

S1=sqrt((syz_1(:)).^2+(sxz_1(:)).^2);

S1_cell=S1(nlist(index_cell, 1));

%% Force Calculation

Meshsize = 16*scal1;

Area=meshsize*meshsize;

Force=Area*S1; totForce=sum (Force);

Cell_force=Area*(S1_cell); totForce_cell=sum (Cell_force);

% % Saving force data

save([Dishn, posn, 'data.mat'], 'xn', 'yn', 'S1', 'S1_cell', 'Force', 'totForce', 'Cell_force', 'totForce_cell')

%% Plotting tractional stress

mx = max(xn)/scal1;

my = max(yn)/scal1;

[xssm, yssm]=meshgrid ([0:1: mx], [0:1:my]);

Zmsh = griddata (xn/scal1, yn/scal1, S1, xssm, yssm);

figure, imshow(zmsh, []); colormap(jet); colorbar;

```

```
hold on, plot(xcell/scal1,ycell/scal1,'r','LineWidth',2);  
  
cbar = colorbar;  
  
set (get(cbar,'ylabel'),'String','Stress [Pa]');  
  
%%
```

## 4.2. Appendix II- ANSYS scripts

### 4.2.1. Model definition

%% Project Name

/TITLE, Substrate

%% Pre-processing

/PREP7

%% Defining the model with the images dimension

ET, 1, SOLID185

KEYOPT, 1, 2, 0

KEYOPT, 1, 3, 0

KEYOPT, 1, 6, 0

MPTEMP,

MPTEMP, 1, 0

MPDATA, EX, 1, 3500

MPDATA, PRXY, 1, 0.4

BLC 4, 0, 0, 9.0667e-5, 7.2e-5, 6.6667e-5

% % Defining the mesh and 3-d meshing the model

AESIZE, ALL, 2.67e-6

MSHKEY, 0

```
MSHAPE, 1, 3d
```

```
CM, Y, VOLU
```

```
VSEL,
```

```
CM, _Y1, VOLU
```

```
CHKMSH,'VOLU'
```

```
CMSEL, S, _Y
```

```
MSHAPE, 0, 3d
```

```
MSHKEY, 1
```

```
VMESH, _Y1
```

```
MSHKEY, 0
```

#### 4.2.2. Applying load on the gel

%% Making tables including the nodes and displacements and apply force on them

```
*dim, Txy, table, 101, 5, 1
```

```
*tread, Txy, 'table1.txt'
```

```
*do,i, 1, 101, 1
```

```
d,Txy(i,1),ux,Txy(i,4)
```

```
d,Txy(i,1),uy,Txy(i,5)
```

```
*enddo
```

```
*dim, loadf, table, 879, 5, 1  
  
*tread, loadf, 'table2.txt'  
  
*do, j, 1, 879, 1  
  
%% Assigning a zero external force  
  
f, loadf(j, 1), fx, 0  
  
f, loadf(j, 1), fy, 0  
  
f, loadf(j, 1), fz, 0  
  
*enddo  
  
%% Fixed gel boundaries  
  
da, 2, ux, 0  
  
da, 2, uy, 0  
  
da, 2, uz, 0
```

### 4.3. Appendix III-Tables: CTFs and cell areas

**Table 4. CTF and cell area for cells grown on 3.5, 7.5 and 20 kPa gel coated with fibronectin**

Young's modulus	3.5 kPa		7.5 kPa		20 kPa	
Fibronectin	CTF [nN]	Area [ $\mu\text{m}^2$ ]	CTF[nN]	Area [ $\mu\text{m}^2$ ]	CTF[nN]	Area [ $\mu\text{m}^2$ ]
1	3.98E+02	2468.25	1.21E+02	1625.1075	84.825	3656.491875
2	8.66E+01	1314	1.76E+01	1419.813	744.75	3194.579
3	4.88E+02	1966.5	5.63E+01	2104.313	465.75	4734.704
4	1.78E+02	1300.5	2.52E+02	3167.375	506.25	7126.593
5	1.29E+02	1140.75	3.47E+02	2020.748	411.75	4546.683
6	2.36E+02	1851.75	5.11E+02	2763.945	436.5	6218.876
7	2.88E+02	1422	3.83E+02	2240.505	113.625	3249.97425
8	1.13E+02	1296	4.05E+02	2279.745	423	5894.67375
9	9.63E+01	1485	2.11E+02	1634.558	57.15	4100.625
10	1.83E+01	1210.5	1.40E+02	1444.433	195.3	1575.45
11	4.19E+02	2288.25	8.66E+01	2619.855	252	5134.64175
12	4.19E+01	945	6.17E+01	1822.5	157.95	2870.4375
13	1.94E+01	805.5	1.73E+01	700.2	206.1	4640.085
14	7.61E+01	1723.5	1.04E+02	2282.063		
15	2.41E+02	4684.5	3.15E+01	1275.75		
16	1.47E+02	1647	1.25E+02	2062.26		
17	5.99E+01	1226.25	4.23E+02	2577.87		
18	5.02E+02	2274.75				
<b>Average</b>	1.97E+02	1725	1.94E+02	2002.414147	311.919	4380.29351
<b>STDEV</b>	160.29	874.55	161.5678	615.435157	202.996	1512.122676

**Table 5. CTF and cell area for cells grown on 3.5, 7.5 and 20 kPa gel coated with collagen**

Young's modulus		3.5 kPa		7.5 kPa		20 kPa	
Collagen	CTF [nN]	Area [ $\mu\text{m}^2$ ]	CTF[nN]	Area [ $\mu\text{m}^2$ ]	CTF[nN]	Area [ $\mu\text{m}^2$ ]	
1	29	2468	188	3756	154	4394	
2	51	1314	137	1216	277	3628	
3	29	1966	63	977	338	4374	
4	20	1300	105	1905	39	2802	
5	72	1141	504	3120	338	4990	
6	31	1852	52	1243	297	2890	
7	27	1422	130	2950	43	1920	
8	32	1296	58	1713	304	3559	
9	28	1485	291	2342	765	5110	
10			344	2066	174	3957	
11			107	2118	326	3050	
12			349	2786			
13			165	1021			
<b>Average</b>	35	1009	192	2094	278	3697	
<b>STDEV</b>	16	327.0	138	874.0	196	986	

#### 4.4. Appendix IV- Sample of analyzed cell images

Sample analyzed cell images with their traction stress distributions. Figure 23: triangular shape cells, Figure 24: spindle shape cells and figure 25: cells with random or small triangular shape on a softer gel.

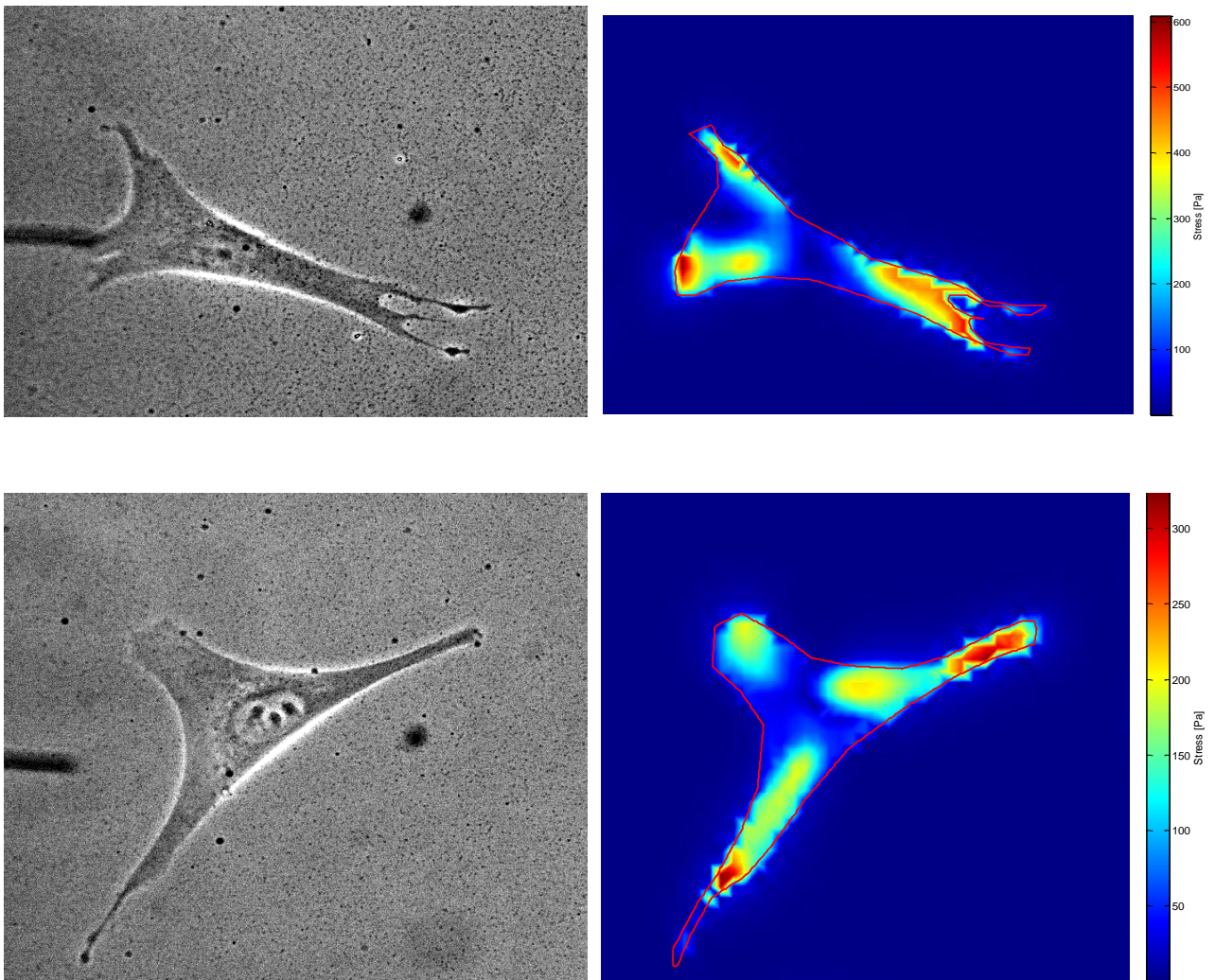


Figure 23. Phase image and tractional stress: Triangular shape cells

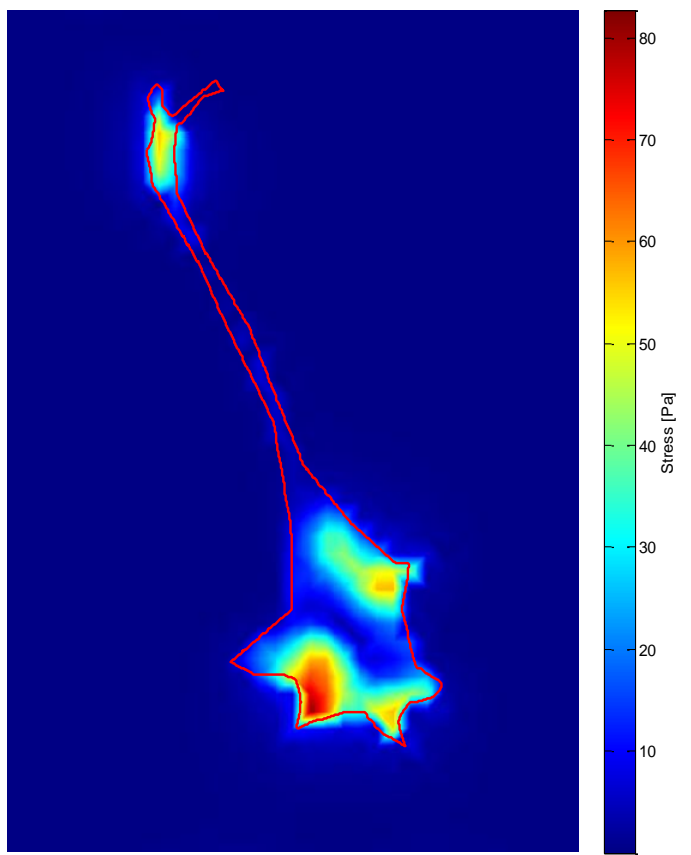
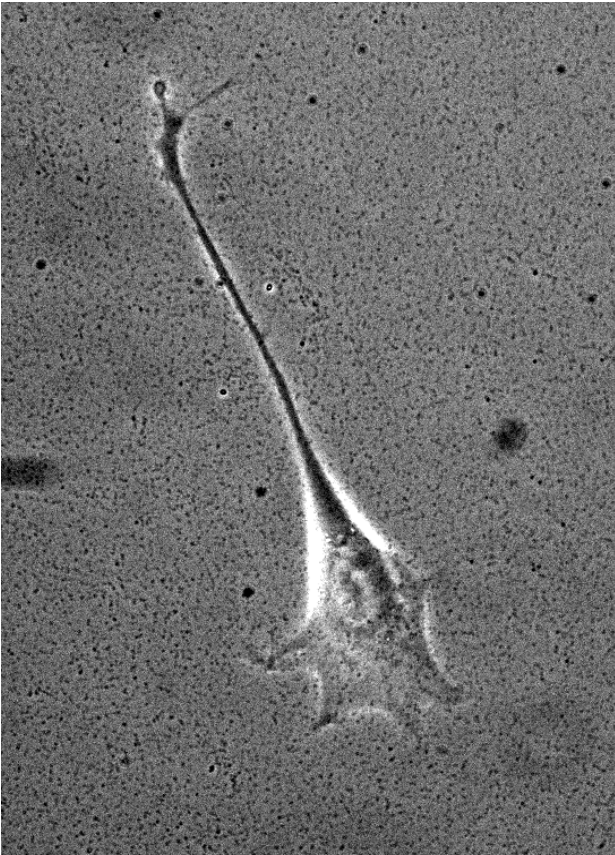
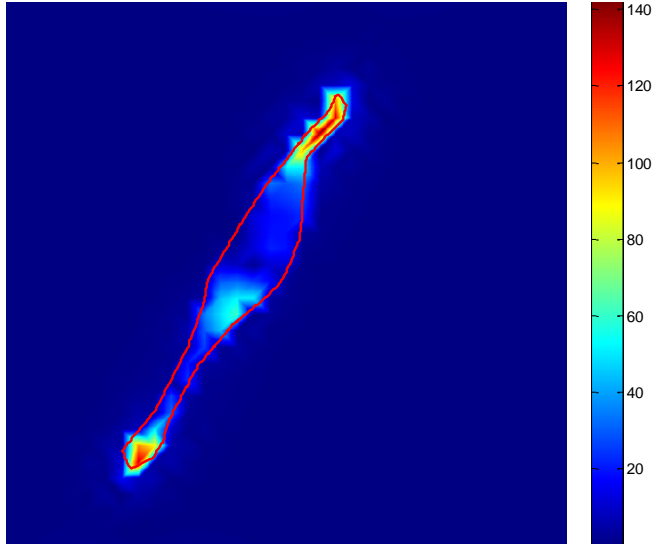
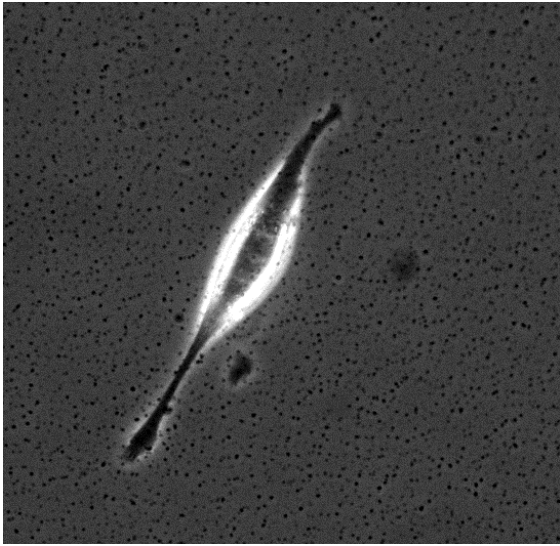


Figure 24. Phase image and tractional stress: Spindle shape cells

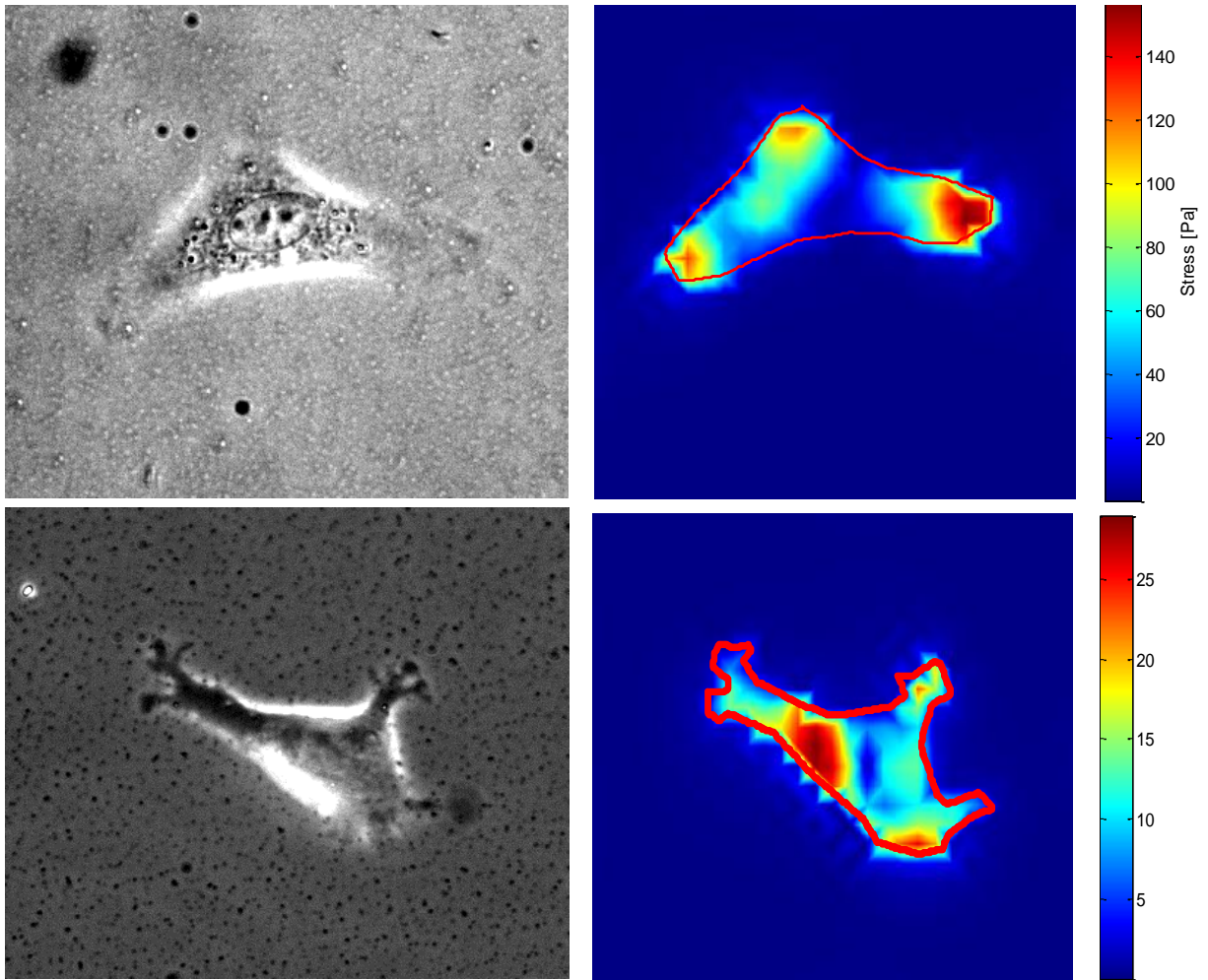


Figure 25. Phase image and tractional stress: Random or small triangular shape cells

## References

1. *Cell type-specific response to growth on soft materials.* **P. C. Georges, Paul A. Janmey.** s.l. : Journal of Applied Physiology, 2005, Vols. 98: 1547-1553.
2. *Integrating cell responses to mechanical stimuli.* **P. A. Janney, C. A. McCulloch.** 2007, cell mechanics, Vols. 9, 1-34, pp. 1-34.
3. *The hard life of soft cells.* **P.A. Janmey, et al.** 8, 2009, Cell Motil Cytoskeleton, Vol. 66, pp. 597-605
4. *Cell mechanics and the cytoskeleton.* **D. A. Fletcher, R. D. Mullins.** 2010. 2010, Nature, pp. 463(7280): 485–492.
5. . *Mechanotransduction – a field pulling together?* **CS.Chen.** s.l. : Journal of Cell Science , 2008, Vols. 121, 3285-3292
6. *Flexible substrata for the detection of cellular traction forces.* **Y. L. Wang, K. A. Beningo.** 2002, Trends in Cell Biology, Vol. 12, pp. 79-84.
7. *The structural and mechanical complexity of cell growth.* **S. Huang, DE. Ingber.** s.l. : Nat. Cell Biol, 1999, Vols. 31–38
8. *Soft biological materials and their impact on cell function.* **I. Levental, PC. Georges , P. A. Janmey :** Soft Matter<sup>1</sup>, 2007; 299–306.
9. *Cell Traction Forces(CTFs) and CTF microscopy applications in musculoskeletal research.* **J. H. Wang.** 2010, Operative Technics in Orthopaedics, pp. 20:106-109
10. *Cell adhesion receptors in mechanotransduction.* **M. A. Schwartz, D. W. DeSimone.** s.l. : Current Opinion in Cell Biology, 2008, Vols. 20: 551-556.
11. *Fibroblasts and myofibroblasts in wound healing: Force generation and measurement.* **B. Liu, J. H. Wang.** s.l. : Journal of tissue viability, 2011, Vols. 20:108-120
12. *Forces and bond dynamics in cell adhesion.* **E. A. Evans, D. A. Calderwood.** 2007, Science , Vol. 316, pp. 1148-1153.
13. *Tissue cells feel and respond to the stiffness of their substrate.* **D. E. Discher et al.,** s.l. : Science, 2005, Vol. 310.
14. *Live cells exert 3-dimensional traction forces on their substrata.* **S. S.Hur et al.** s.l. : Cellular and Molecular Bioengineering , 2009, Vols. 2: 425-436.

15. *Cell traction force and measurement methods*. **J. H. Wang, J. Lin**. 2007, *Biomechan Model Mechanobiol* , Vol. 6, pp. 361-371.
16. "*Integrins in Mechanotransduction*". **A. Katsumi, et al**. 2003, *Journal of Biological Chemistry* 279 (13), pp. 12001–4.
17. *Integrins*. **B. Malgorzata, et. al**. 1 , s.l. : *Cell Tissue Res*, 2010, Springer, *Adv Protein Chem*, Vols. 339: 269–280.
18. *Crystal structure of the A domain from the  $\alpha$  subunit of integrin CR3 (CD11b/CD18)*. **J. Lee, P. Rieu, M. A. Arnaout, R. Liddington**. 1995, *Cell* , Vol. 80, pp. 631–638.
19. *Integrin activation*. **D. A. Calderwood**. 2004, *J. Cell Sci.* , Vol. 117, pp. 657-666.3.
20. *Structural basis for allostery in integrins and binding to fibrinogen-mimetic therapeutics*. **T. Xiao, J. Takagi, B. S. Collier, J. H. Wang, T. A. Springer**. s.l. : *Nature*, 2004, Vols. 432, 59-67.
21. *The three-dimensional structure of integrins and their ligands, and conformational regulation of cell adhesion*. **T. A. Springer, J. H. Wang** . s.l. : *Advanced Protein Chemistry*, 2004, Vols. 68, 29-63
22. *Crystal structure of the extracellular segment of integrin  $\alpha$  Vbeta3 in complex with an Arg-Gly-Asp ligand*. **J. P. Xiong, T. Stehle, R. Zhang, A. Joachimiak, M. Frech, S. L. Goodman, M. A. Arnaout**. 2002, *Science* , Vol. 296, pp. 151-155
23. *Integrin ligands at a glance*. **J. D. Humphries, A. Byron, M. J. Humphries**. 2006, *Cell Sci.*, Vol. 119, pp. 3901-3903.
24. *Cold Spring Harb Perspective*. **I. D. Campbell, M. J. Humphries**. 3, 2011, *Biology* , Vol. 3
25. *A multi-station culture force monitors system to study cellular contractility*. **B. H. Campell, W.W. Clark and J. H. Wang**. 1, 2003, *Journal of Biomechanics* , Vol. 36, pp. 137-140.
26. *A micropatterning and image processing approach to simplify measurement of cellular traction forces*. **S. R. Polio et al**. 2012, *Acta Biomaterialia* , Vol. 8, pp. 82-88.
27. *A novel functional assessment of the differentiation of micropatterned muscle cells* . **B. Li et al**. 2008, *Journal of Biomechanics* , Vol. 41, pp. 3349-3353.
28. *Probing cellular traction forces by Micropillar Arrays* **I. Scheon et al**. 5, 2010, *Nanoletters* , Vol. 10, pp. 1823-1830.
29. *Cells lying on a bed of microneedles: An approach to isolate mechanical force* . **J. L. Tan et al**. 2003, *Current issue* , Vol. 100, p. 1484:1489.
30. *Stress at the Cell-to-Substrate Interface during Locomotion of Fibroblasts*. **Y.Wang, M. Dembo** 1999, *Biophysical Journal* , Vol. 76, pp. 2307-2316

31. *Traction fields, moments, and strain energy that cells exert on their surroundings.* **J. P. Butler et al.** 2002, *American Journal of Physiol Cell Physiol* , Vol. 282 , pp. 595-605.
32. *Determining substrate displacement and cell traction fields – a new approach.* **Z. Yang et . al.** 2006, *Journal of Theoretical Biology* , Vol. 242, pp. 607-616
33. *Flexible substrata for the detection of cellular traction forces .* **K. A. Beningo and Yu-Li Wang.** 2002, *Trends in Cell Biology*, Vol. 12, pp. 79-84
34. *Tissue cells feel and respond to the stiffness of their substrate.* **Dennis E. Discher et al.** 5751, 2005, *Science.* , Vol. 310, pp. 1139-43
35. *Adhesion of chicken hepatocytes to polyacrylamide gels derivatized with N acetylglucosamine.* **Schnaar RL, Weigel PH, Kuhlenschmidt MS, Lee YC, and Roseman.** 1978, *J Biol Chem* , Vol. 253, pp. 7940–7951
36. *Cell locomotion and focal adhesions are regulated by substrate flexibility.* **Y., Pelham RJ Jr and Wang.** 1997, *Proc Natl Acad Sci USA* , Vol. 94, pp. 13661–13665.
37. *Image processing, analysis and machine vision,* . **M. Sonka et al.** 1993, Vol. 265, p. 555.
38. *Substrate stiffness and cell area predict cellular traction stresses in single cells and cells in contact .* **Reinhart, J. P. Califano and C. A.** 2010, *Cellular and Molecular Biology* , Vol. 3, pp. 68-75
39. *Cell movement is guided by the rigidity of the substrate.* **Y. Wang, M. Dembo.** 1, 1999, *Biophysical Journal*, Vol. 79, pp. 144-152.
40. *Traction stresses and translational distortion of the nucleus during fibroblast migration on a physiologically relevany ECM mimic.* **Z. Pan et. al.** : *Biophysical Journal*, 2009, Vols. 96: 4286-4298
41. *Absence of Filamin A prevents cells from responding to stiffness gradients on gels coated with collagen but not fibronectin;* **J. Fitzroy, Byfield et al.** 2009, *Biophysical Journal*, Vol. 96, pp. 5095-5102
42. *How cells sense extracellular matrix stiffness: a material's perspective.* **B. Trappmann, CS. Chen.** s.l. : *Current Opinion in Cell Biology*, 2013, Vol. 24.
43. *Cell Traction Forces Direct Fibronectin Matrix Assembly.* **C. A. Lemmon et al.** (21), 2009, Vols. 96:729–738.